PB80-202690

# A Tunable Diode Laser Stack Monitor for Sulfuric Acid Vapor

Laser Analytics, Inc.
Bedford, MA

Prepared for

Environmental Sciences Research Lab.
Research Triangle Park, NC

TYPING GUIDE SHEET

PB80-202690

EPA 600/2-80-174
August 1980

# A TUNABLE DIODE LASER STACK MONITOR FOR SULFURIC ACID VAPOR

by

Edwin F. Pearson
Arlan W. Mantz
Laser Analytics, Inc.
Bedford, Massachusetts 01730

68-02-2990

Project Officer

Roosevelt Rollins
Emission Measurement and Characterization Division
Environmental Sciences Research Laboratory
Research Triangle Park, North Carolina 27711

ENVIRONMENTAL SCIENCES RESEARCH LABORATORY
OFFICE OF RESEARCH AND DEVELOPMENT
U.S. ENVIRONMENTAL PROTECTION AGENCY
RESEARCH TRIANGLE PARK, NORTH CAROLINA 27711

REPRODUCED BY
NATIONAL TECHNICAL
INFORMATION SERVICE
U.S. DEPARTMENT OF COMMERCE
SPRINGFIELD, VA. 22161

## DISCLAIMER

This report has been reviewed by the Environmental Sciences Research Laboratory, U.S. Environmental Protection Agency, and approved for publication. Approval does not signify that the contents nessarily reflect the views and policies of the U.S. Environmental Protection Agency, nor does mention of trade names or commercial products constitute endorsement or recommendation for use.

BEGIN FIRST LINE OF TEXT HERE
TYPING GUIDE SHEET
CENTER OF PAGE
TOP OF IMAGE AREA
DROPPED HEAD: BEGIN SECTIONS HERE


## ABSTRACT

A prototype instrument for in situ monitoring of sulfuric acid vapor in industrial smoke stacks has been developed. The method of detection is dual wavelength differential absorption in the infrared. Two tunable diode lasers (TDL) are locked to two specific frequencies which provide analytical and background absorption information. The difference between the analytical and background absorbance yields the net absorbance due to sulfuric acid.

Calibration of the monitor depends upon a precise determination of the differential absorption coefficient for the analytical and background frequencies. Measurements made as a part of this program yield a value of $12.2 \times 10^{-4}$ $ppm^{-1}$ $m^{-1}$ and tend to resolve the discrepencies between previously published values. Temperature gradients in the absorption cells severely influenced previous measurements.

The monitoring system was field tested at a 650 MW electrical generation plant burning high sulfur oil of Venezuelan origin. The excess air supplied to the boiler combustion chamber was varied from 0.5 to 1.5 percent. Measured baseline concentrations of sulfuric acid ranged from 3 to 25 ppm showing a critical dependence upon the conditioning of the boiler surfaces. As the excess air was stepped from 0.5 to 1.5 percent the average measured increase in concentration was 39 ppm. The system gave consistent results during the brief test period.

This report was submitted in fulfillment of Contract No. 68-02-2990 by Laser Analytics, Inc. under the sponsorship of the U.S. Environmental Protection Agency. This report covers the period September 26, 1978 to March 1, 1980, and work was completed as of December 18, 1979.


BEGIN LAST LINE OF TEXT
BOTTOM OF IMAGE AREA OUTSIDE DIMENSION FOR TABLES AND ILLUSTRATIONS
3/8"



PAGE NUMBER
EPA-287 (Cin.)
(4-76)

BEGIN FIRST LINE OF TEXT HERE
TYPING GUIDE SHEET
CENTER OF PAGE
TOP OF IMAGE AREA
DROPPED HEAD; BEGIN SECTIONS HERE

CONTENTS

Abstract . . . . . iii
Figures . . . . . v
Tables . . . . . viii
1. Introduction . . . . . 1
2. Conclusions . . . . . 3
3. Recommendations . . . . . 5
4. Design Concepts . . . . . 7
Dual Wavelength Differential Absorption . . . . . 7
Wavelength Lock and Modulation . . . . . 10
5. Optical System . . . . . 15
Dual Laser Mounts . . . . . 15
Optical Pallet. . . . . 15
Laser Tests . . . . . 21
Stability Tests . . . . . 25
Stack Coupling Flanges . . . . . 25
6. Electronics and Data Acquisition . . . . . 30
7. $H_2SO_4$ Calibration Cell . . . . . 33
Design Considerations . . . . . 33
Calibration Measurements . . . . . 37
8. Field Test . . . . . 43
Site Selection . . . . . 43
Test Plan . . . . . 43
Test Conditions . . . . . 44
Results . . . . . 45
Summary of Results . . . . . 51
References . . . . . 52
Appendix . . . . . 53
Interference Absorption Spectra . . . . . 54

BEGIN LAST LINE OF TEXT HERE
BOTTOM OF IMAGE AREA OUTSIDE DIMENSION FOR TABLES AND ILLUSTRATIONS
3/8"



PAGE NUMBER
EFA-287 (Cin.) (4-76)

FIGURES


| Number | | Page |
|---|---|---|
| 1 | Schematic of $H_2SO_4$ stack monitor optics and electronics | 8 |
| 2 | Calculated $H_2O$ interference in the region of the analytical frequency | 11 |
| 3 | Calculated $CO_2$ interference in the region of the analytical frequency | 11 |
| 4 | Calculated $H_2O$ interference in the region of the background frequency | 12 |
| 5 | Calculated $CO_2$ interference in the region of the background frequency | 12 |
| 6 | Calculated $NO_2$ interference in the region of the analytical frequency | 13 |
| 7 | Maximum temperature separation in dual laser cold head (TCR) versus operating temperature | 16 |
| 8 | Thermal regulation power as a function of temperature separation in dual laser cold head with no laser load | 17 |
| 9 | Etalon effects observed in optical system, a) calibration cell to TCR window, b) local detector to return detector, c) local detector to local retroreflector to return detector | 18 |
| 10 | Detectivity maps of typical detector elements | 20 |
| 11 | $H_2SO_4$ monitor optical system schematic | 22 |
| 12 | $H_2SO_4$ monitor optical system photograph | 23 |
| 13 | Results of laboratory stability tests of optical system before pinhole filter installation | 26 |
| 14 | Laboratory stability test results for optical system after pinhole installation | 27 |
| 15 | Stack coupling flange and windows | 28 |
| 16 | Laser control and data acquisition system block diagram | 31 |

| | | |
|---|---|---|
| 17 | Photograph of electronics and data acquisition system | 32 |
| 18 | $H_2SO_4$ calibration cell diagram showing liquid azeotrope reservoir, absorption paths and copper heating jacket | 34 |
| 19 | $H_2SO_4$ calibration cell pallet optical diagram | 35 |
| 20 | Photograph of $H_2SO_4$ calibration cell attached to monitor optical pallet | 36 |
| 21 | Calculated and measured absorbances of calibration cell as a function of reservoir temperature. Cell temperature 192°C | 40 |
| 22 | Calculated and measured absorbances of calibration cell as a function of reservoir temperature. Cell temperature 206°C | 41 |
| 23 | Calculator printout of measurements on Tuesday, October 2. Instrument sensitivity setting are given in the left column and test results are in the middle and right columns. Results given in absorbance units. ppm($H_2SO_4$) = 150 (a.u. - 0.36) | 46 |
| 24 | Measurements results for October 3. Arrows indicate excess air increases. Blank areas are periods when the monitor was in an internal test configuration. Time scale begins at 10:14 hours | 47 |
| 25 | Control room record of excess air levels, October 3. Units are in percent. Left trace applies to duct monitored | 48 |
| 26 | Measurement results for October 4. Arrows indicate excess air increase and decrease. Time scale begins at 09:44 hours | 49 |
| 27 | Control room record of excess air levels, October 4. Left trace applies to duct monitored. Units are excess air in percent | 50 |
| A-1 | Calculated $H_2O$ background absorption spectrum for 5 meter path at 473°K, 12% $H_2O$ (91 Torr) with data taken from the Air Force line listing in the 880 $cm^{-1}$ region | 54 |
| A-2 | Calculated $CO_2$ background absorption spectra for 5 meter path at 523°K and 473°K with a pressure of 114 Torr in the 880 $cm^{-1}$ region | 55 |
| A-3 | Calculated $H_2O$ background absorption spectra for 5 meter path at 743°K, 91 Torr in the 960 $cm^{-1}$ region | 56 |
| A-4 | Calculated $CO_2$ background absorption spectra for 5 meter path at 523°K and 473°K with a pressure of 114 Torr in the 960 $cm^{-1}$ region | 57 |

A-5 Calculated $NO_2$ background absorption spectra for 5 meter path at 423°K, 25 ppm concentration in the 880 $cm^{-1}$ region . . . . 58

A-6 Calculated $CO_2$ background absorption spectra for 5 meter path at 473°K, 114 Torr in the 960 $cm^{-1}$ region . . . . . 59

A-7 Calculated $H_2O$ background absorption spectra for 5 meter path at 473°K, 91 Torr in the 950 $cm^{-1}$ region . . . . . 60

A-8 Calculated $H_2O$ background absorption spectra for 5 meter path at 473°K, 91 Torr in the 970 $cm^{-1}$ region . . . . . 61

A-9 Calculated $CO_2$ background absorption spectra for 5 meter path at 473°K, 114 Torr in the 970 $cm^{-1}$ region . . . . . 62

## TABLES


| Number | | Page |
|---|---|---|
| 1 | Acronym Key . . . . . | 9 |
| 2 | Laser Operating Points . . . . . | 24 |
| 3 | Calibration Cell Measurement Results . . . . . | 37 |

## SECTION 1

## INTRODUCTION

Acid rain with its harmful effects on plant and animal life has focused considerable interest in the sources of sulfur and nitrogen oxides. Atmospheric emissions of these substances come from the burning of fossil fuels, the smelting of sulfide ores, volcanoes and other natural sources. Human activities have made significant changes on a continental scale and these effects are expected to rise further with increased dependence upon coal and lower quality oil.

In the combustion of sulfur containing fuels the primary product is sulfur dioxide which can be oxidized and hydrolized in the atmosphere to form sulfuric acid. However, stationary sources such as electric power generation plants emit sulfuric acid directly from their stacks. As much as ten percent of the sulfur may be converted to sulfur trioxide either by atomic oxygen in the combustion zone or by efficient catalysis on heavy metal contaminents in the fuel. At moisture levels above four percent and temperatures in the range of 150-200°C, theoretical models indicate that sulfuric acid vapor should predominate over sulfur trioxide.

To better understand the factors controlling acid emissions from stacks an in situ, real time monitoring system for suifuric acid is needed. Current measurements are confined to wet chemical methods which require long sampling times, are sensitive to operator techniques, and may not discriminate sufficiently between sulfuric acid and sulfur trioxide.

This report describes the development and testing of a spectroscopic instrument designed for continuous monitoring of sulfuric acid vapor concentrations. Although spectroscopic measurements of species such as $SO_2$ and CO are routine, sulfuric acid presents a far more difficult problem. This molecule displays no sharp absorption features in the IR and is not amenable to detection systems based upon gas filter correlation. In general, fixed frequency laser techniques are limited by interference from the absorption lines of water, carbon dioxide and other species. Laser Analytics' approach to the measurement problem is a dual wavelength tunable diode laser (TDL) system capable of selectively avoiding interference lines and discriminating against scattering from particulates and dirty optics.

Monitoring sulfuric acid by spectroscopic techniques requires that the infrared absorption spectrum be well characterized. Laboratory measurements are difficult to obtain because of the very low vapor pressure at room temperature and the dissociation, equilibrium and chemical attack problems in a heated cell. Quantitative low resolution (~1 $cm^{-1}$) spectra were obtained by Burch et al at Aeronautronic Ford[1] and by Majkowski[2] at the General

Motors Research Laboratory. The two absorption bands of interest occur at 1220 $cm^{-1}$ and 880 $cm^{-1}$. Peak absorption coefficients for each of these bands were of the order of 2-5 $cm^{-1}$ $atm^{-1}$. While these absorption strengths appear adequate for infrared monitoring of sulfuric acid in stack gas the task would have been simplified by the location of sharp spectral features. Eng et al.[3,4] at Laser Analytics, Inc. performed high resolution (.0001 $cm^{-1}$) measurements on both the 1220 and 880 $cm^{-1}$ bands. Both low pressure and atmospheric pressure observations were made. No resolved structure was observed in either case. Measured peak absorption coefficients for the 1220 $cm^{-1}$ and 880 $cm^{-1}$ bands were found to 6.5 and 6.9 $cm^{-1}$ $atm^{-1}$, respectively. Analysis of the data in these experiments included the effects of dissociation of the sample when the observation cell was maintained at a temperature higher than the liquid reservoir. Reanalysis of Majkowski's data on this basis gave a value in very good agreement with Eng's measurements.

Majkowski[5] has reported a new value for the peak absorption coefficient for the 1220 band which is four times greater than his first published value[2]. This sharp increase upon remeasurement was attributed to improved experimental technique, particularly the elimination of hot spots, and to a re-evaluation of the equilibrium controlled dissociation of the $H_2SO_4$ in the absorption cell.

## SECTION 2

## CONCLUSIONS

1. A tunable diode laser differential absorption instrument has been demonstrated to be a promising approach to the search for a reliable sulfuric acid vapor monitor. The first continuous, real time measurement of sulfuric acid concentration as a function of combustion conditions has been realized.

2. Stability studies which included over 600 hours of laboratory measurements demonstrated that drifts in indicated response could be kept within 0.01 absorbance units over a three hour period. The limitations were found to be primarily related to detector motion in the focal plane, depending upon $LN_2$ levels in the detector dewars. Spatial variations in the element responsivity, V/W, combined with the relative motion of the detector elements produce unequal responses for the two laser images. This is seen as system drift.

3. The system zero level is established through relatively straightforward but precise alignment procedures. However, the introduction of windows in the analytical path was found to increase the uncertainty in the zeroing. This uncertainty would be completely eliminated if the measurements were made through a purgeable pipe.

4. Measurements of the peak absorption coefficient of the 880 $cm^{-1}$ band of $H_2SO_4$, made with the laboratory calibration cell, yielded a value of $13.3 \times 10^{-4}$ $ppm^{-1}$ $m^{-1}$. Discussions with previous investigators and reexamination of some of their data leads us to conclude that the earlier studies were adversely affected by hot spots and large thermal gradients in the absorption cell.

5. Field testing of the monitor confirmed the feasibility of the design concept. A one week test program on the stack of a 650 MW electrical generation plant yielded the first continuous record of sulfuric acid emissions. The unit tested was burning high sulfur oil of Venezuelan origin. Minimum vapor concentrations measured on the first two test days ranged between 3 and 8 ppm. On the third and final test day, the lowest level recorded was 25 ppm. On two test days, combustion conditions were varied by increasing the excess air input from 0.5 to 1.5 percent. Measured increases in acid vapor concentrations were 32 ppm and 46 ppm.

6. The feasibility of dual laser monitoring was confirmed. Simultaneous operation of two tunable diode lasers (TDL) in one temperature controlled refrigerator (TCR) was demonstrated for the first time in a practical measurement system.

7. Optical feedback could be completely eliminated from the system. The significant steps taken to eliminate feedback were rotation of the detector off the optical axes, offset return of the laser beam and spatial filtering.

8. Linelocking of the lasers assured reliable, unattended operation. This technique was found to be stable and rugged under field conditions.

## SECTION 3

## RECOMMENDATIONS

1. Optical determination of the zero level for the monitor was achieved in the laboratory through reasonably straightforward alignment procedures. Problems with this technique appeared when the stack windows were included in the system. These windows exhibited an intrinsic differential attenuation of 0.36 absorbance units between the infrared frequencies used for monitoring. However, a slight wedging in the windows led to apparent values of differential absorption which were critically dependent upon window orientation. Thus, the major contribution to the uncertainty in the system zero in the field was a window effect which could not independently be checked once the instrument was mounted on the stack.

We, therefore, recommend the use of a purgeable pipe for future measurements. The high precision of the dual wavelength monitoring instrument can be realized with a purgeable path. The system is capable of making corrections for apparent differential absorption when used with a purged pipe. In the purged pipe configuration the system zero could be routinely confirmed to within the system noise level of approximately 0.005 absorbance units.

2. An experimental program should be carried out on the stack simulator at the EPA Environmental Sciences Research Laboratory. This would serve to establish the limitations of zeroing procedures. In addition, the introduction of $CO_2$, $H_2O$, $NO_2$, and other interfering species at various concentrations and temperatures would demonstrate the immunity of the monitor to interference from these abundant stack gas components.

3. Essential to the successful design of the monitor was the prototype dual laser temperature controlled refrigerator (TCR). Two improvements in its design are needed to make the monitor more versatile. First, the maximum attainable temperature separation between the lasers should be increased. This would relax the tight constraints on laser selection and lessen the chance for delays in laser replacement. Second, the laser mounts could be designed to permit the installation of up to four lasers in the TCR. Only two lasers would operate simultaneously but the additional lasers used separately or as a pair would permit rapid switching to measurements of other gases. Installation of additional lasers would also reduce the per channel cost of the system.

4. Although the system has been designed to monitor $H_2SO_4$ which has absorption bands with no find structure it could easily be equipped with lasers suitable for monitoring species such as CO, $SO_2$, $NO_x$, and $HNO_3$. Only minor

software changes would be required for measurements based on sharp spectral line features.

5. A modest research effort to evaluate the feasibility of mounting detector elements inside the TCR would be desirable. This would eliminate the requirement for supplying cryogens to the detectors. It is also anticipated that such an arrangement would reduce the magnitude of detector element displacements and thus lead to improved system stability.

6. A smaller and more rugged optical pallet should be developed. The weight would be reduced through the use of relieved panels instead of solid aluminum plate. Experience with the present system has shown that the pallet area can be reduced by 25 percent. A 40 percent reduction would be possible if the detectors were mounted inside the TCR.

7. The volume and weight of the electronics and data systems could be reduced at least 40 percent by eliminating redundant functions and unnecessary features. Digital control would provide more reliable unattended operation and permit automatic switching of experimental conditions.

8. Because of the large increase in the measured value of the $H_2SO_4$ absorption coefficients further refinements in intensity measurements are warranted. It has been shown that serious errors can result from large temperature variations over the reservoir, connecting line and absorption cell. In the present work, differences as small as two degrees celsius were accommodated without difficulty. Future measurements should be made with total temperature variations not greater than two degrees.

## SECTION 4

## DESIGN CONCEPTS

### DUAL WAVELENGTH DIFFERENTIAL ABSORPTION

The principle of dual wavelength differential absorption is best illustrated by referring to Figure 1 and the acronym key given in Table 1. The combined outputs of the two TDL's at infrared frequencies $\nu_A$ and $\nu_B$ are divided by beamsplitter $BS_2$. The fraction which is directed to detector $D_L$ via mirror $M_2$ establishes the local sample of the laser power. The transmitted fraction passes across the stack to a retroreflector and returns to $BS_2$ where it is directed to the return detector $D_R$ via mirror $M_3$. Laser signal intensities are related to measured intensities by the relations:

$$I'_{AL} = k_1 I_{AL}$$
$$I'_{AR} = k_2 I_{AR}$$
$$I'_{BL} = k_3 I_{BL}$$
$$I'_{BR} = k_4 I_{BR} \qquad (1)$$

where the k's include beamsplitter and other optical efficiencies. Absorptions at the two IR frequencies can be expressed as

$$\alpha_A L + \sigma_A = \ell n \left[I'_{AL}/I'_{AR}\right] \qquad (2)$$

$$\alpha_B L + \sigma_B = \ell n \left[I'_{BL}/I'_{BR}\right] \qquad (3)$$

where $\alpha_A$ and $\alpha_B$ are the $H_2SO_4$ vapor absorption coefficients at the two respective IR frequencies; L is the absorption path length and $\sigma_A$, $\sigma_B$ include absorption due to interfering molecular species, particulates and optics. Subtracting Equation (3) and (2) yields:

$$(\alpha_A - \alpha_B)L + (\sigma_A - \sigma_B) = \ell n \left(I'_{AL} I'_{BR}/I'_{AR} I'_{BL}\right) \qquad (4)$$

$$C_{H_2SO_4} = (S_A - S_B)^{-1} L^{-1} \left\{\ell n \left[k(I'_{AL} I'_{BR}/I'_{AR} I'_{BL})\right] - (\sigma_A - \sigma_B)\right\} \qquad (5)$$

where $k = (k_1 k_4)/(k_2 k_3)$, $C_{H_2SO_4}$ is the sulfuric acid concentration and $S_A$ and $S_B$ are the absorption coefficients per unit $H_2SO_4$ vapor concentrations at the analytical and background IR frequencies $\nu_A$ and $\nu_B$ respectively. In principle, the normalization constant k should be unity if the beamsplitter and

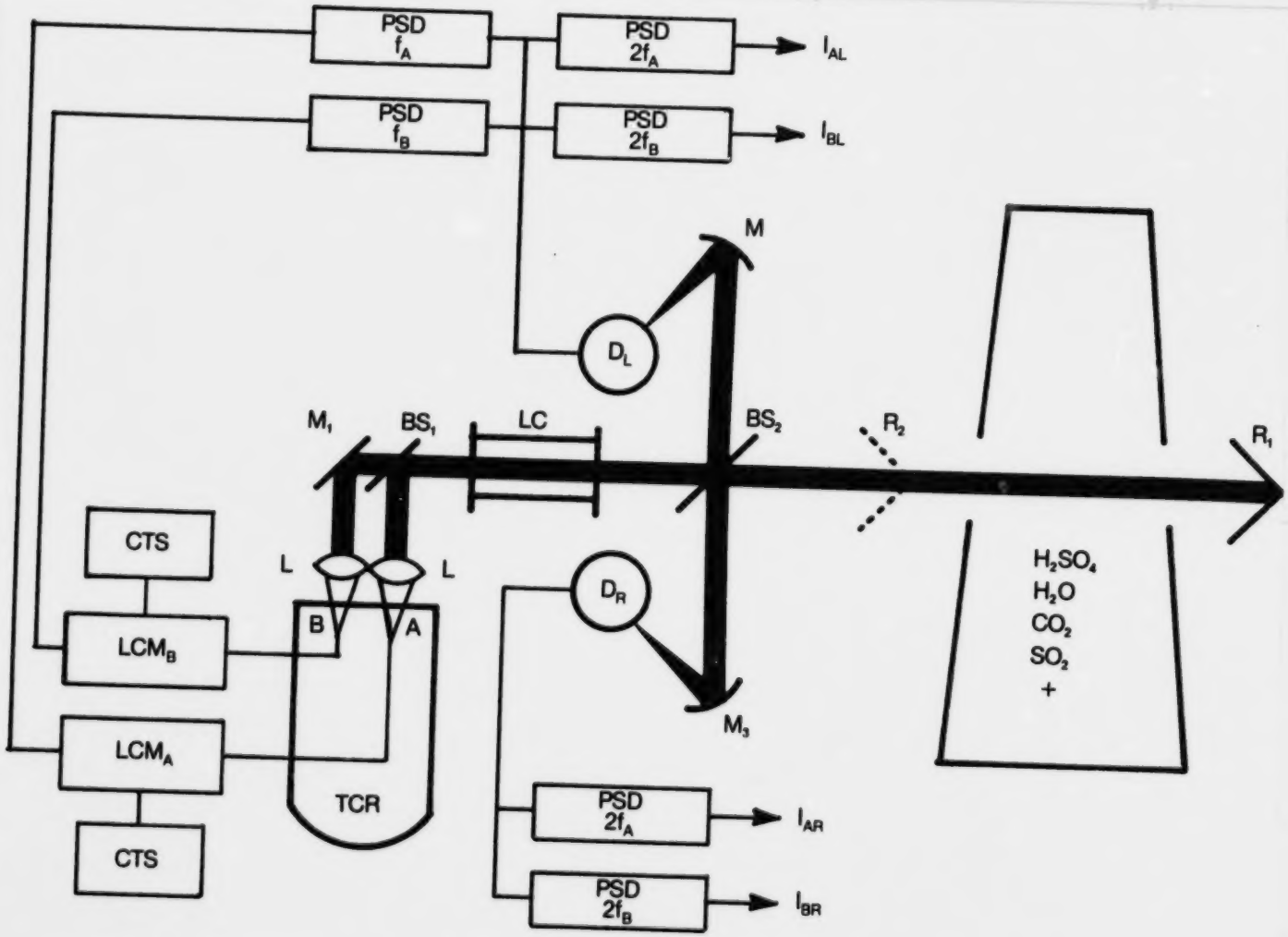


Figure 1. Schematic of $H_2SO_4$ stack monitor optics and electronics.

TABLE 1. ACRONYM KEY

| | |
|---|---|
| A | -subscript-Analytical laser frequency |
| $A_1$, $A_2$ | Aperture |
| ADC | Analog to Digital Converter |
| B | -subscript-Background laser frequency |
| $BS_1$, $BS_2$ | Beamsplitter |
| CTS | Cryogenic Temperature Stabilizer |
| $D_L$, $D_R$ | Detector |
| $f_A$, etc | laser modulation frequency |
| $I_{AL}$, etc | laser intensity |
| He Ne | Helium Neon laser |
| L | -subscript- local |
| L | lens |
| LCM | Laser Control Module |
| $M_1$, etc | Mirror |
| MP | Mirror-Pellicle mount |
| PH | Pinhole |
| PSD | Phase Sensitive Detector (Lock-in amplifier) |
| R | -subscript- Return |
| $R_1$, etc | Retroreflector |
| TCR | Temperature Controlled Refrigerator (cold head) |
| TDL | Tunable Diode Laser |

optical efficiencies are independent of infrared frequency. In practice it is found to be within a few percent of unity for a properly aligned system.

Calibration of the measurement depends upon the difference in the absorption coefficients at the two IR frequencies. Discussion of the determination of this value is given in Section 7.0. The result, $(S_A - S_B) = 12.2 \times 10^{-4}$ ppm$^{-1}$ m$^{-1}$ implies that to achieve a detection sensitivity of 5 ppm-m the instrument must register a change in differential absorbance of 0.006.

Effects of interfering species, $(\sigma_A - \sigma_B)$, are minimized by a careful selection of monitoring frequencies. Figures 2-6 show calculated spectra for $H_2O$, $CO_2$ and $NO_2$ in the regions of the analytical 882.029 cm$^{-1}$, and background, 962.160 cm$^{-1}$, frequencies. These plots were generated for the condition of 15% $CO_2$, 12% $H_2O$ and 25 ppm $NO_2$ over a path of 5 meters at 150°C, the temperature of the stack gases encountered in the field test. From the figures the total interfering absorbances are found to be .007 and .006 at the analytical and background frequencies. The net differential absorbance, $(\sigma_A - \sigma_B)$, is then 0.001. This illustrates the effectiveness of the high resolution, tunable laser system in reducing the effects of interfering molecular species. Particulate matter will also absorb and scatter infrared radiation. However, over the wavelength separation of the two laser probes there is no significant differential absorption.

Extended studies of interference absorption lines in the analytical and background regions are given in Appendix A. An inspection of these figures clearly shows that the number of interfering spectral features is non-negligible. Low resolution techniques cannot adequately exclude these effects, because they effectively integrate over a large number of lines.

## WAVELENGTH LOCK AND MODULATION

The key design concept which has made dual wavelength monitoring with TDL's feasible is Laser Analytics' modulation and line locking technique.[6] This eliminates the need for a mode separating monochromator and permits reliable unattended operation of the lasers.

The TDL's are independently tuned by varying the current from the Laser Control Modules (LCM). If the applied current is given by:

$$J = J_1 + J_2 \sin(2\pi f t) \tag{6}$$

where $J_1$ is the DC component and the second term represents a dither current, then the laser output frequency will have the approximate form:

$$\nu = \nu_1 + \Delta\nu_1 \sin(2\pi f t) \tag{7}$$

Where $\Delta\nu_1$ is the dither frequency magnitude. When this frequency modulated radiation is passed through a cell containing a low pressure gas which has a strongly absorbing spectral feature centered at $\nu_1$ only a laser mode as $\nu_1$ will be amplitude modulated. The laser frequency (wavelength) lock loop is completed by a phase sensitive detector (PSD) tuned to the modulation fre-

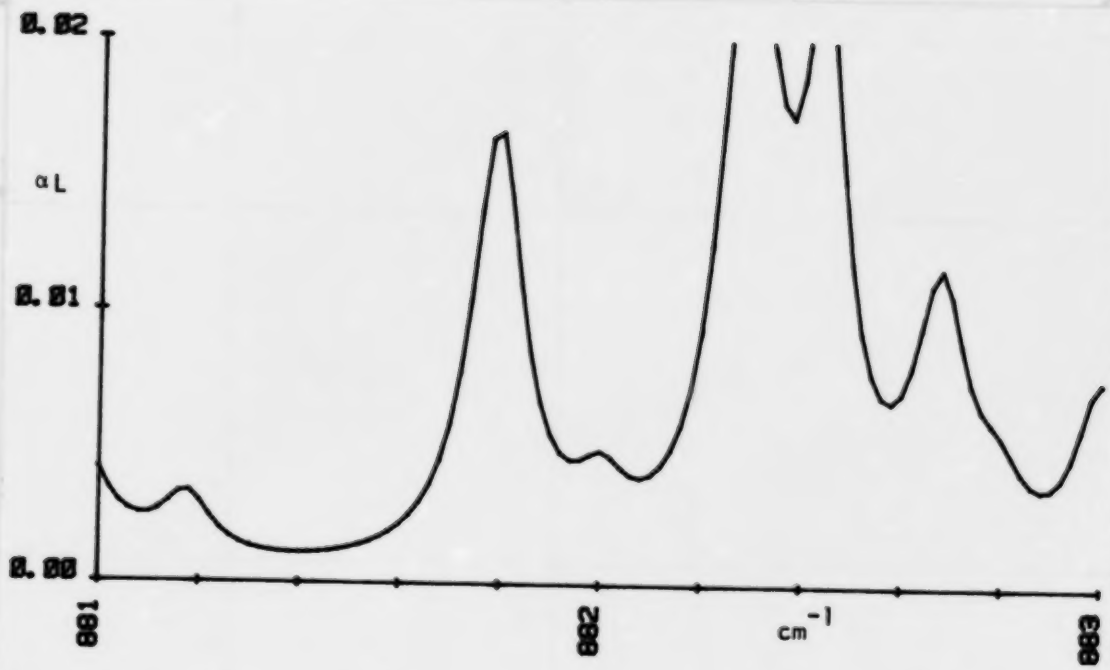


Figure 2. Calculated $H_2O$ interference in the region of the analytical frequency.

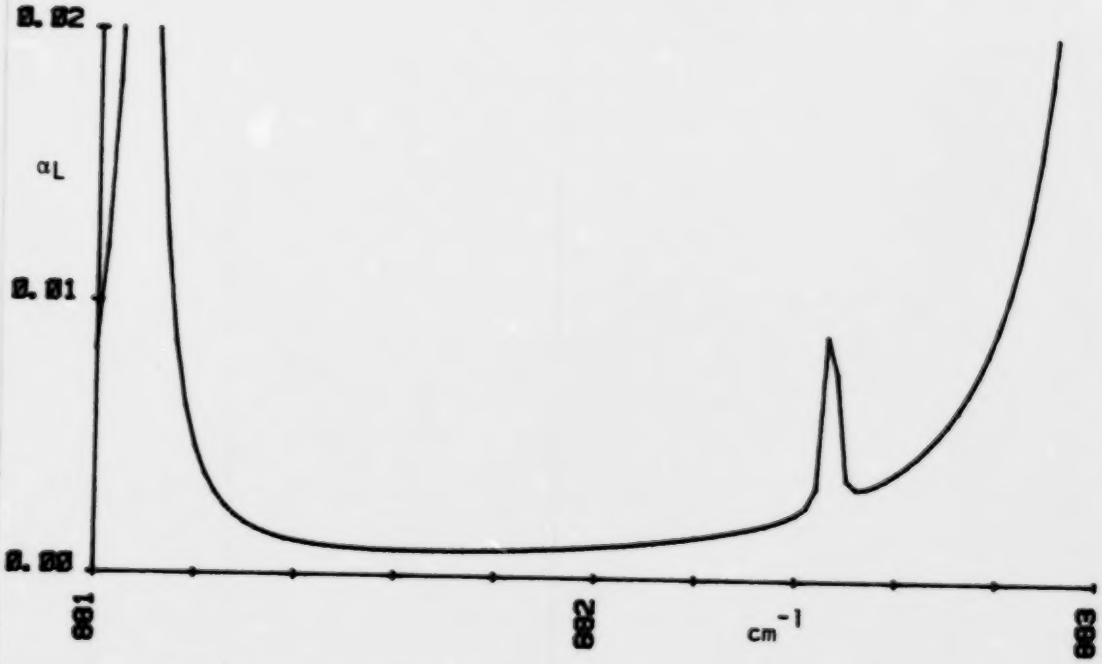


Figure 3. Calculated $CO_2$ interference in the region of the analytical frequency.

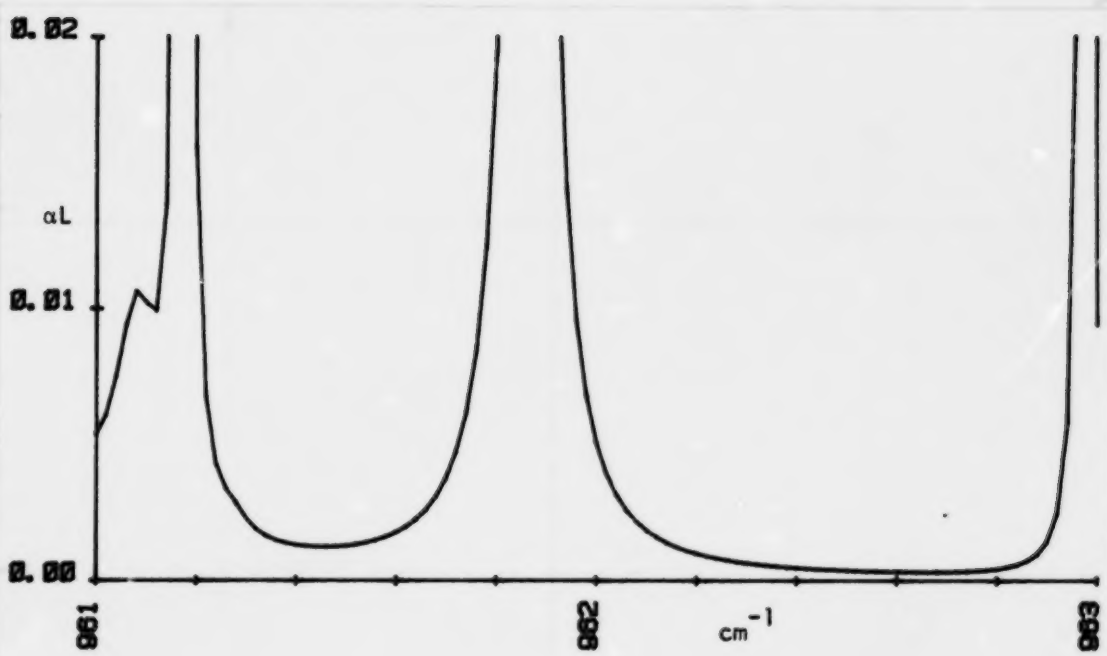


Figure 4. Calculated $H_2O$ interference in the region of the background frequency.

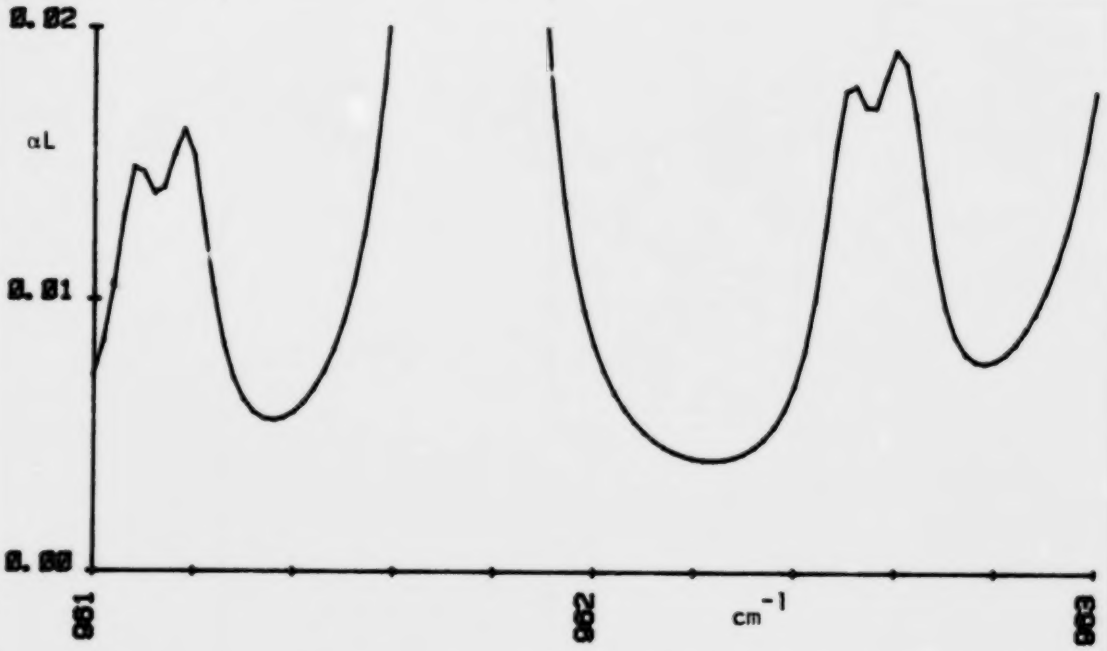


Figure 5. Calculated $CO_2$ interference in the region of the background frequency.

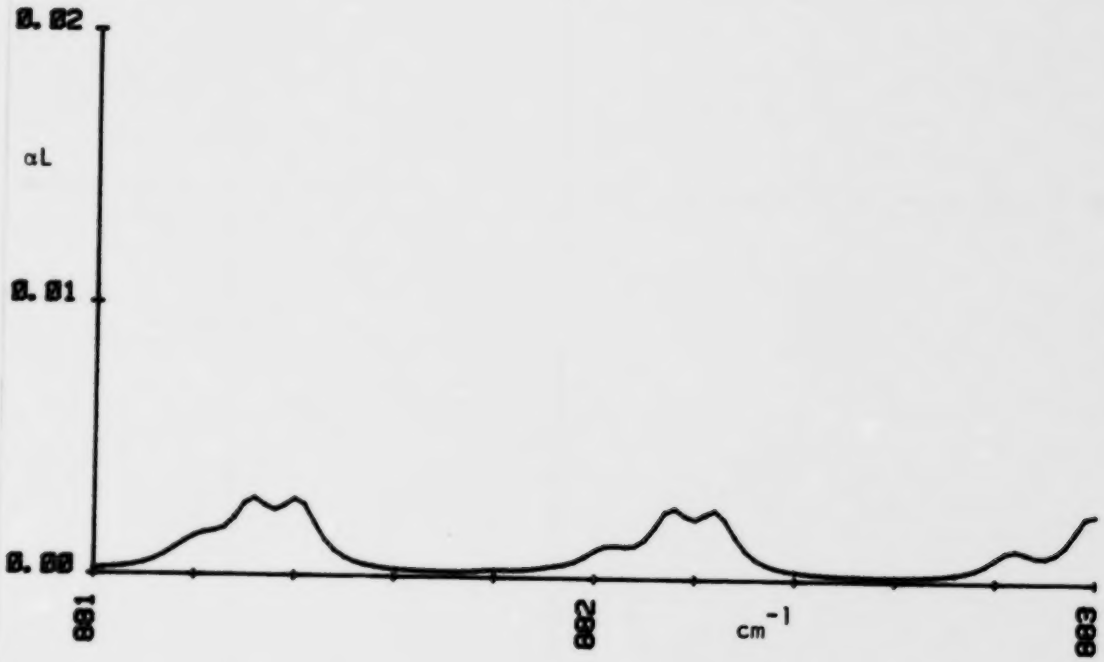


Figure 6. Calculated $NO_2$ interference in the region of the analytical frequency.

quency, f. Output of the PSD, which corresponds to a first derivative of the absorption profile, provides the correction signal to the LCM.

Analysis of the laser output power shows that the dither across the lock cell absorption line produces an amplitude modulation at the frequency 2f. Another PSD tuned to this second harmonic will then monitor the relative received laser power.

Referring to Figure 1, it is seen that the complete system involves two infrared detectors, $D_L$ and $D_R$, and six PSD's. The local detector, $D_L$, supplies input to both the lock loop (1f) and signal level (2f) PSD's. Because the lasers are modulated at two distinct frequencies the PSD's serve to separate the multiplexed information. The two PSD's connected to the return detector, $D_R$, function in the same manner.

The line lock and modulation cell can be filled with any gases which provide suitable absorption features at the desired wavelengths. Optimum modulation is achieved with a Doppler limited absorption line and a dither excursion which is approximately 1.2 times the Doppler halfwidth.

Outputs of the PSD's, $I_{AL}$, $I_{BL}$, $I_{AR}$ and $I_{BR}$ are digitized and supplied to a calculator which averages the results and calculates the $H_2SO_4$ concentration from Equation (5). Results are printed at operator definable intervals.

Selection of the lock lines to be employed is a compromise among the stable gases which have strong, sharp, assignable absorptions falling in the available interference free wavelength regions (Appendix A). Initially lines of $NO_2$ and $NH_3$ at 881.410 and 962.254 $cm^{-1}$ respectively were selected to control the analytical and background infrared frequencies. Early tests indicated that improved operation could be obtained by switching to a mixture of $NH_3$ and OCS. The final selections, employed both in laboratory and field testing, were the R(62) transition of the $\nu_1$ band of OCS at 882.029 $cm^{-1}$ and $^sQ$ (9,9) transition of the $\nu_2$ band of $NH_3$ at 962.160 $cm^{-1}$. These choices do not represent a unique compromise but rather proved to be effective and convenient. The selection can also be influenced by operating temperature constraints of the dual laser Temperature Controlled Refrigerator (TCR).

## SECTION 5

## OPTICAL SYSTEM

### DUAL LASER MOUNTS

Simultaneous operation of two TDL's was achieved through the design of a dual laser Temperature Controlled Refrigerator (TCR). This modification of a standard Laser Analytics' product was developed under a NSF program for long path monitoring.[7] Two independently regulated laser mounts were attached to the heat sink of a closed cycle cryogenic refrigerator.

Attainable temperature separation of the two lasers as a function of the set temperature of one of them is illustrated in Figure 7. This plot was obtained by adjusting the Cryogenic Temperature Stabilizer (CTS) for one laser position and following the unregulated (lower) temperature of the other position. Maximum temperature separation with both lasers operating will be reduced and will depend upon the specific laser characteristics. At the time of the field test, the lasers were operated with a separation of 4.3°K. Figure 8 is a plot of the power provided to each of the temperature regulating heaters as a function of the separation of the two temperatures. For this case, $T_1$ was held fixed at 32°K. It is seen that the operation is not quite symmetrical because of an unequal thermal resistance between each laser position and the common heat sink.

### OPTICAL PALLET

The original optical configuration conformed to the schematic concept illustrated in Figure 1. The two laser beams were combined by a mirror-beamsplitter assembly directly in front of the lasers. The collimated radiation passed through the lock cell and was divided by a beamsplitter, $BS_2$, which served both to provide detector $D_L$ with local reference intensities and to direct the returning radiation to detector $D_R$. This direct retroreflected approach proved vulnerable to standing wave or etalon effects which responded sensitively to mechanical and thermal displacements. The net effect was instability in the zero baseline of the instrument. In extreme cases, feedback of the laser radiation occured causing large instabilities in laser output.

Three examples of etalon effects are shown in Figure 9. These fringes were identified with the following paths: a) calibration cell to TCR window, b) local detector to return detector, c) local detector to local retroreflector to return detector.

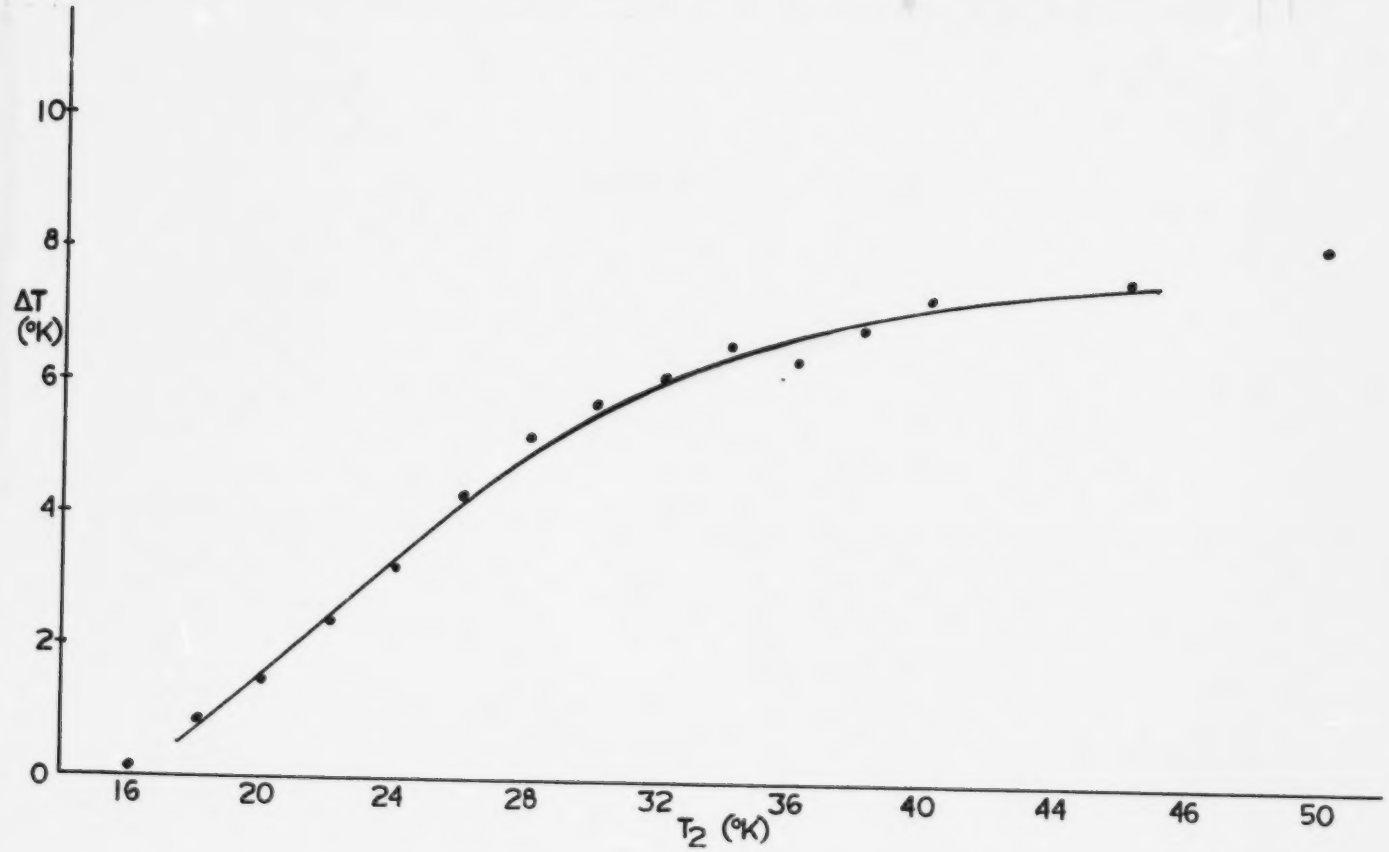


Figure 7. Maximum temperature separation in dual laser cold head (TCR) versus operating temperature.

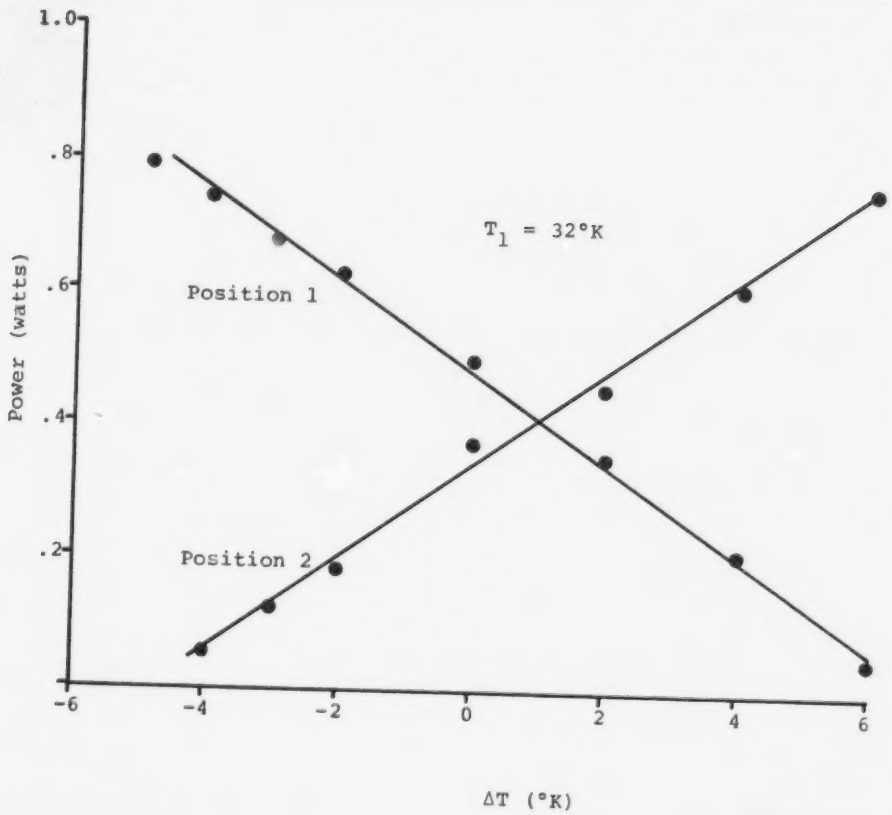


Figure 8. Thermal regulation power as a function of temperature separation in dual laser cold head with no laser load.

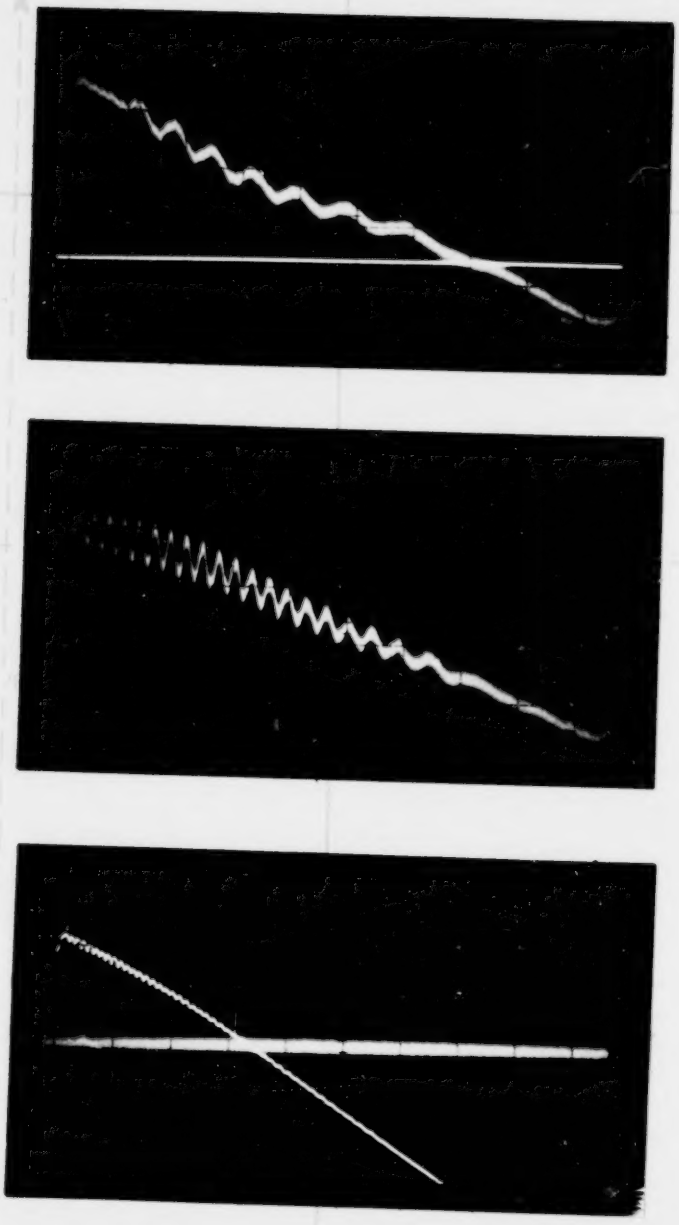

Figure 9. Etalon effects observed in optical system, a) calibration cell to TCR window, b) local detector to return detector, c) local detector to local retroreflector to return detector.

To completely eliminate feedback and other etalon effects, the direct retroreflected return beam was changed to a staggered configuration. The beam was directed off center onto the corner cube retroreflector so that it returned on a displaced, parallel path. An added benefit was that all of the returned radiation could be brought to the return detector. In the original configuration beamsplitter $BS_2$ directed only 35 percent of the returning radiation to the detector. The detectors were also repositioned so that the element normals were skewed about 10° relative to the optic axis.

Considerable effort was devoted to defining alignment procedures which would lead to reliable determination of the zero level for the instrument. Referring to Figure 1 and Equation 5 this is seen to mean that in the absence of $H_2SO_4$ absorption, the value of the normalization constant k given by

$$k^{-1} = I_{AL} I_{BR} / I_{AR} I_{BL} \tag{8}$$

should be the same for a beam returned from a remote retroreflector $R_1$ and for the case where another retroreflector, $R_2$, short circuits the path. In other words, it is necessary to insure that the value of k obtained from $R_2$, which is on the optical pallet, represents the correct normalization for the distant reflector, $R_1$.

The energy emitted from a TDL is generally contained within an f:1 cone. However, the distribution of energy within this cone is not homogeneous; the radiation tends to be confined to separate narrow filaments within the larger cone. These filaments can be emitted from separate regions of the laser crystal which may represent an effective object with typical dimensions of the order of a few hundred microns. These characteristics have two important consequences. First, the finite effective object size determines the residual divergence of a collimated beam. Second, the filamentary composition of the emissions yields inhomogeneous beams after collimation.

The residual divergence is of the order of 1 milliradian for the optical system. Over a path of several meters, the expanded beam becomes large enough to vignette on the optical apertures. If the radiation pattern were homogeneous, this would not necessarily be a serious problem. The actual power distribution, however, can lead to unequal losses in the received power from each laser and hence, a change in the effective normalization. Additionally, with spatially inhomogeneous beams it is not possible to find an optimum signal level in scanning an image across the detector, because the image plane has hot spots. The severity of this problem was not fully appreciated prior to the initiation of this program.

A further problem arises when the characteristics of the infrared detector elements are considered. These one millimeter square elements are larger than the images produced by the focusing mirrors $M_2$ and $M_3$. However, the response over the surface of the elements is not uniform. Recent studies at Laser Analytics, Inc. performed under a separate contract[8] have provided mappings of detector elements. Results for the detectors employed in the $H_2SO_4$ monitor are shown in Figure 10.

S/N 3776

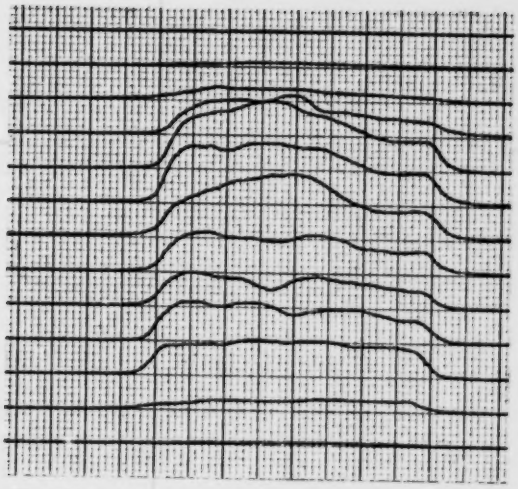

S/N 3775

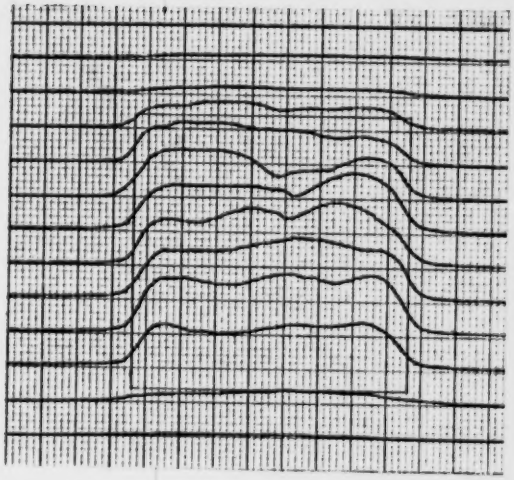

Figure 10. Detectivity maps of typical detector elements.

These contours reveal differences of a factor of two or greater. When one considers the superimposed images of the two lasers on the return detector, it is easy to see that small displacements which come with the switching from the near to the far retro mirror can result in sizeable changes in the ratioed intensities.

Consideration of the homogeneity problems and unsatisfactory results in our efforts to obtain reliable normalization procedures suggested that the laser outputs should be spatially filtered. This was accomplished through the incorporation of a pinhole in the system. The final optical layout is illustrated in Figure 11. The lenses, L, image the laser outputs on the pinhole, PH. The mirror, $M_1$, and beamsplitter, $BS_1$, serve to combine the two beams. Radiation emerging from the pinholes is directed by mirror $M_2$ to an off-axis parabaloid (OAP), $M_3$, which serves to collimate the beam. After traversing the lock/modulation cell, LC, a sample of the beam is directed to $M_7$ which is an OAP that images on the detector element of $D_L$.

The probe beam continues from $BS_2$ to $M_5$ where it is directed through the stack and returns to $M_6$. The OAP, $M_8$, images onto detector $D_R$ to complete the optical circuit. A helium-neon laser, HeNe, can be coupled into the optical path through a removable mirror-pellicle module, MP. The visible beam is used to align both the components on the pallet and the retroreflector. Figure 12 is a photograph of the complete optical pallet. All components can be identified by reference to Figure 11.

## LASER TESTS

TDL's can be tailored to emit in desired wavelength regions by control of the energy gap through adjustment of the chemical composition of ternary semiconductor materials. Once fabricated a diode's precise emission wavelength within the operating region is a function of temperature. Regulation of both the laser crystal temperature and the injection current are required to maintain emission at a given wavelength. Each laser has its own peculiar wavelength-temperature-current characteristics which may vary with age and cycling between cryogenic and room temperatures.

Selection of appropriate lasers begins by applying the criterion that a given pair operate within the temperature separation constraints of the dual laser TCR. A selected pair must next be characterized with a monochromator. The laser beam is deflected from the pallet after it has passed through the lock cell and sent to the monochromator. The appropriate lock lines are located and the current and set point temperature of each LCM and CTS are recorded. The lasers should be temperature cycled and the procedure repeated to insure reproducibility.

Several lasers were tested in the course of this effort. Final selection was determined primarily on the basis of cycling stability. Table 2 summarizes the operating condition of the selected lasers over a ten week period ending with the field test. Temperatures are recorded in terms of CTS sensor voltage readings which are reproducible to greater accuracy than the absolute temperature calibration. Different polarities of the two diodes merely reflects differences in the details of the fabrication process. Both

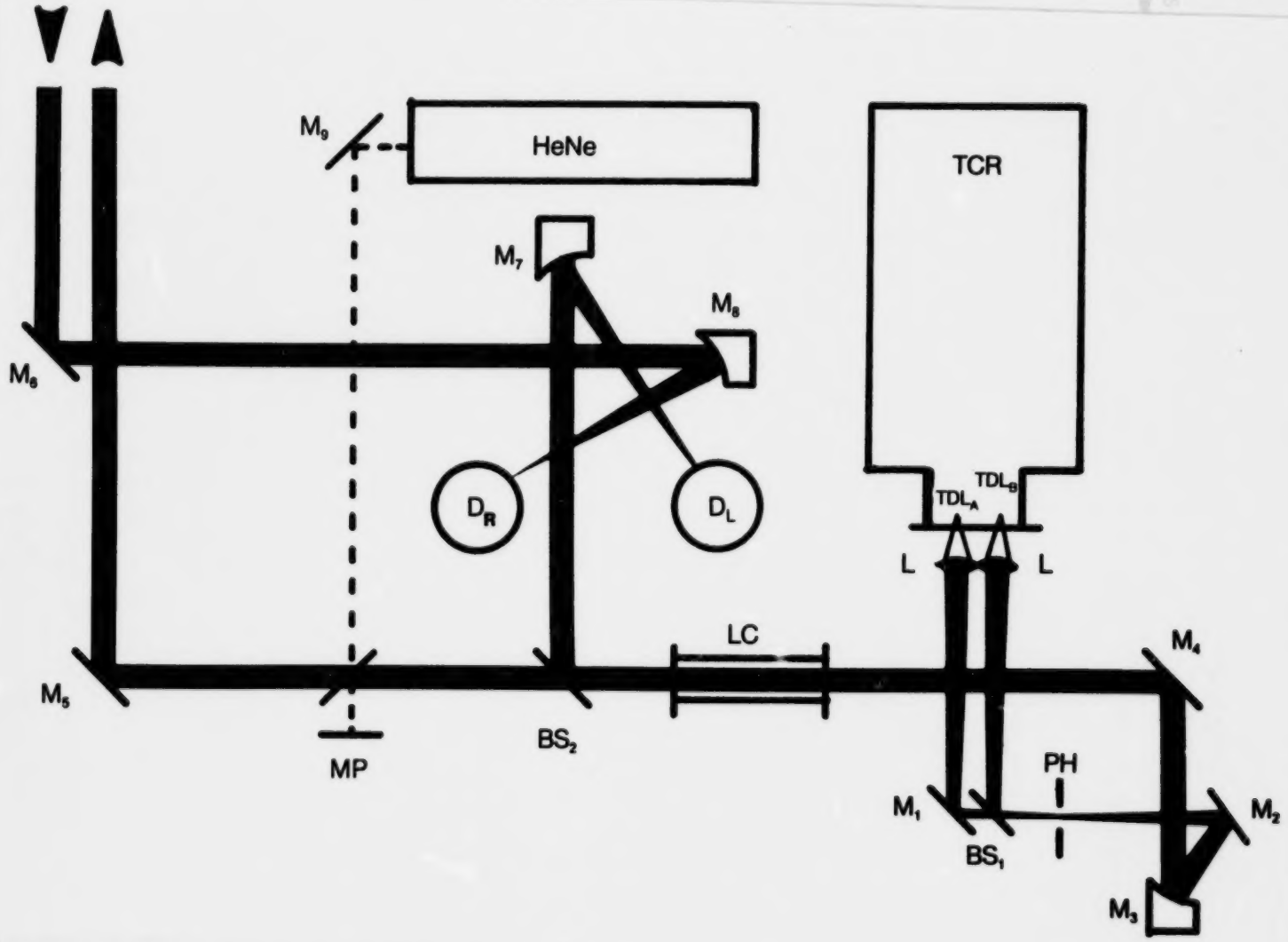


Figure 11. $H_2SO_4$ monitor optical system schematic.

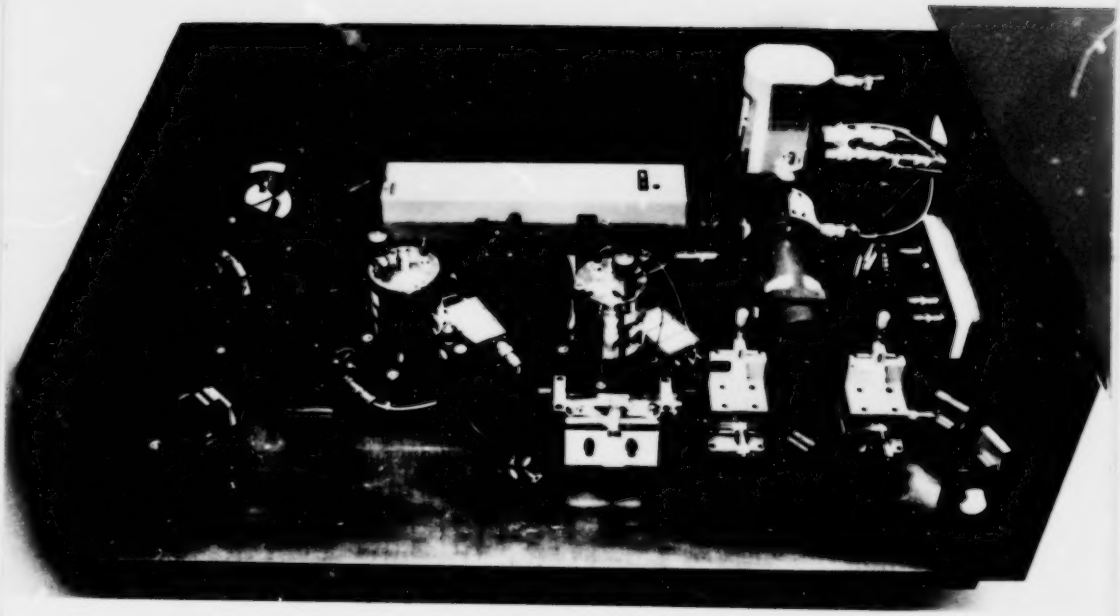

Figure 12. $H_2SO_4$ monitor optical system photograph.

## TABLE 2. LASER OPERATING POINTS

| | S/N 9054-8<br>881.410 $cm^{-1}$ | | S/N 9178-31<br>962.254 $cm^{-1}$ | |
|---|---|---|---|---|
| Date | T | I | T | I |
| 19 July | 1.0788 | -0.873 | 1.0664 | 1.730 |
| ---------- cycled ---------- | | | | |
| 5 Aug | 1.0788 | -0.833 | 1.0660 | 1.390 |
| | 1.0783 | -0.810 | 1.0677 | 1.715 |
| 8 Aug | 1.0790 | -0.842 | NO CHANGE | |
| 12 Aug | 1.0791 | -0.840 | 1.0677 | 1.707 |
| ---------- cycled ---------- | | | | |
| 13 Aug | 1.0791 | -0.851 | 1.0677 | 1.715 |
| | 1.0783 | -0.809(improved operation) | | |
| ---------- cycled ---------- | | | | |
| 20 Sept | 1.0803 | -0.924 | | |
| 25 Sept | 1.0803 | -0.930 | 1.0686 | 1.675 |
| ---------- cycled ---------- | | | | |
| 2 Oct | 1.0800 | -0.926 | 1.0684 | 1.668 |
| 3 Oct | 1.0803 | -0.945 | 1.0686 | 1.667 |
| 4 Oct | 1.0801 | -0.926 | 1.0686 | 1.668 |

diodes were operated with injection currents near threshold in order to reduce the number of modes emitted.

## STABILITY TESTS

Continuous monitoring sensitivity is limited by long term internal drift in the instrument. For a continuous monitor, frequent adjustment and calibration should not be necessary. An intensive effort was, therefore, made to identify and remove sources of instability. More than 600 hours of stability tests were conducted following assembly of the instrument. These tests led to improvements in pallet rigidization, removal of sources of optical feedback, strengthening and replacement of some optical mounts, spatial filtering as well as development of reliable alignment procedures.

Laser amplitude variations are effectively removed from the system response by the ratioing scheme. No drifts in the PSD receivers or other electronics were of consequence. System limiting stability in the current optical configuration is associated with the cooling of the infrared detectors. The detector elements are mounted on the tips of liquid nitrogen dewars. Changes in the coolant level cause displacements of the elements. The laser images consequently move across the elements. Both vignetting and the uneven response of the elements cause these motions to be recorded as output variations. These effects are most pronounced when coolant is added and may display recovery times of several minutes. Careful focusing and precise alignment are essential to the reduction of these effects.

Figure 13 shows the level of performance achieved prior to the incorporation of the pinhole. Each strip covers 3.3 hours and shows variations within 0.01 absorbance units (1 au = 820 ppm-m). These tests were run in the laboratory with the retroreflector at a distance of 3 meters from the optical pallet. Stability results obtained following the spatial filtering modification are shown in Figure 14. The sharp deviation in the first hour resulted from replenishing the coolant in the dewar.

In general, our results with the pinhole in place were more predictable than those without a pinhole, and stability was typically better than 0.01 absorbance units on time scales of 1/2 hour.

## STACK COUPLING FLANGES

The flange and window assemblies were specifically tailored to the requirements of the field test site. Access to the stack was through a 4-inch diameter slotted pipe. The pipe was terminated with gate valves at each end. The valves had standard schedule 150, ten inch diameter flanges.

To avoid deposits on the windows, a short section of pipe containing an aluminum honeycomb material was designed to attach to the gate valve. This material would inhibit diffusion of soot and droplets toward the windows and also act as a field of view limit. Cell size was 0.125 inches and cell depth was 3 inches. Alignment was made through two threaded shafts in the outer flange. The complete assembly is illustrated in Figure 15.

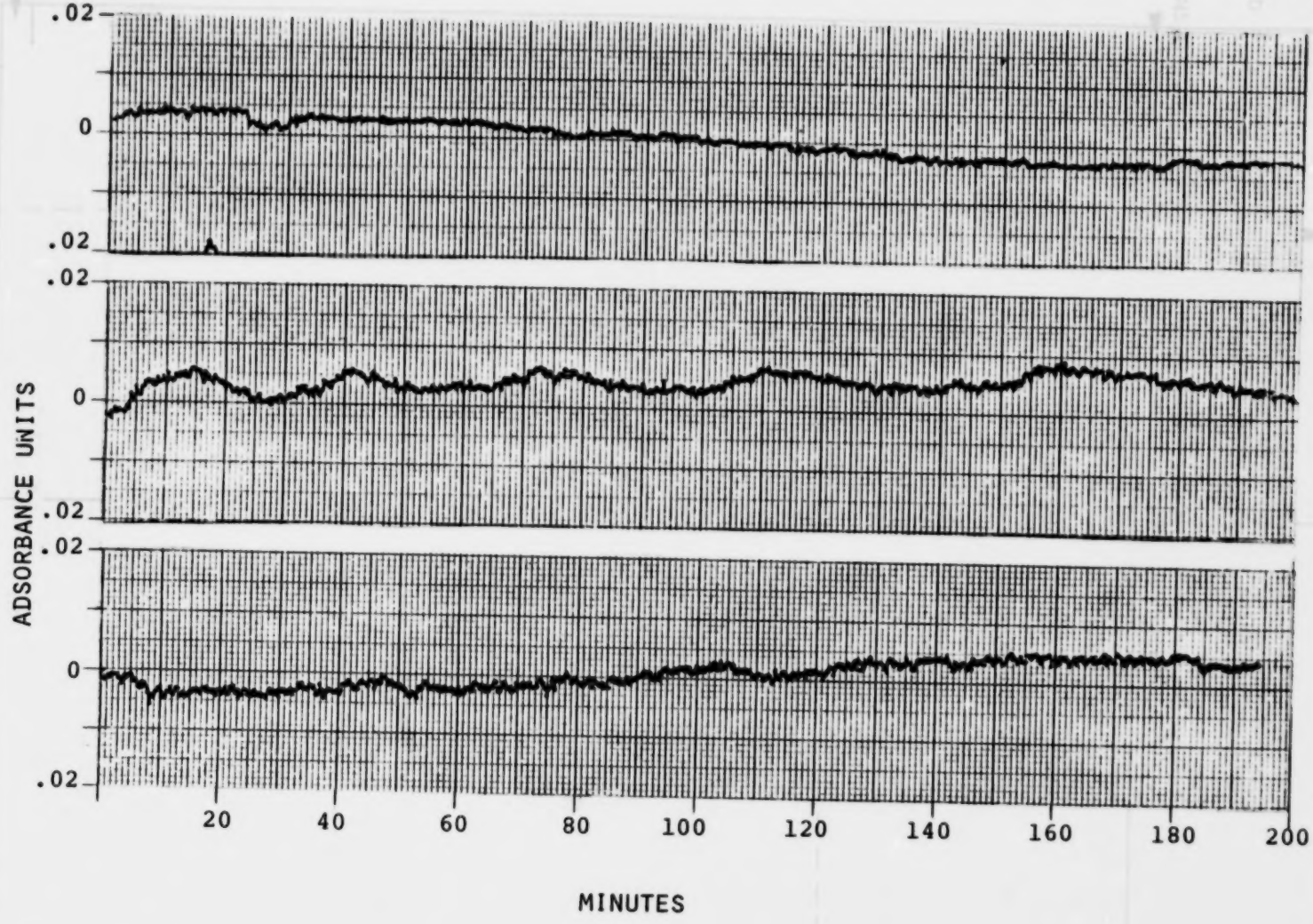


Figure 13. Results of laboratory stability tests of optical system before pinhole filter installation.

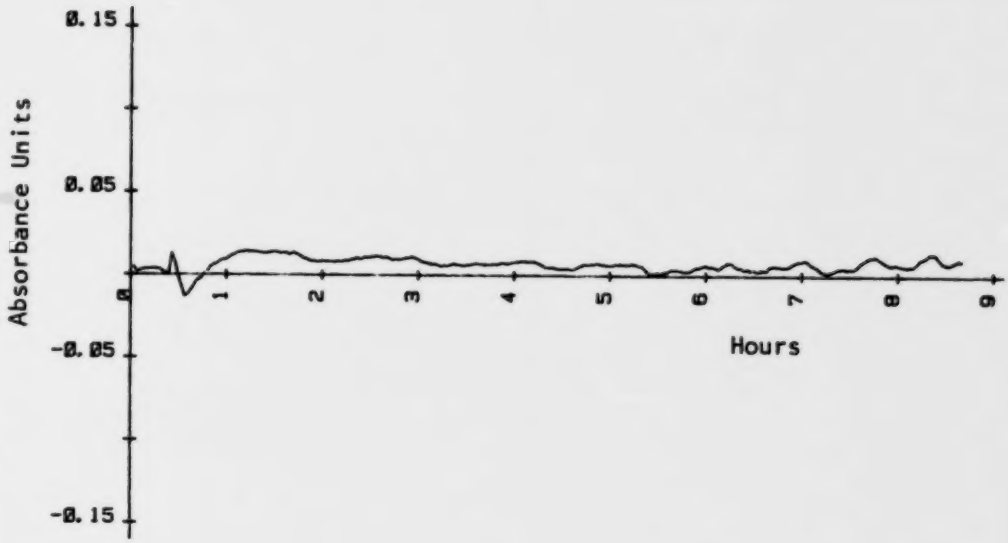


Figure 14. Laboratory stability test results for optical system after pinhole installation.

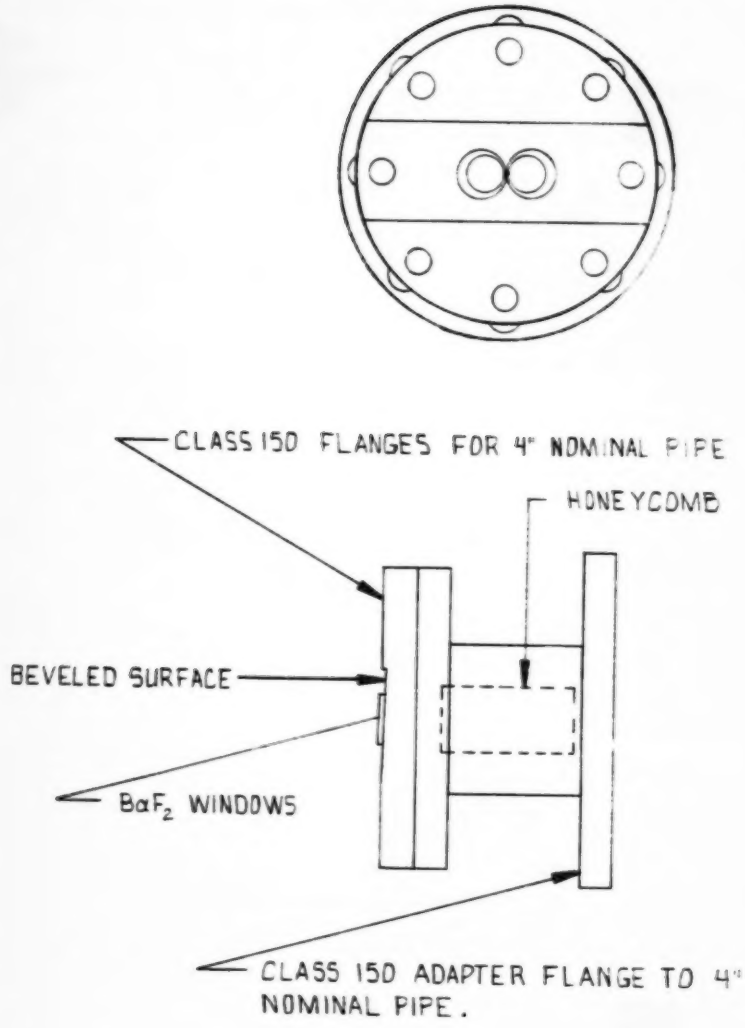


**Figure 15. Stack coupling flange and windows.**

Laboratory tests of this system showed that it introduced greater attenuation of the laser beam than expected. It was difficult to adjust and interfered with visual alignment. Prior to the field test, the honeycomb was removed. The only window contamination encountered in the field test was liquid condensation on one side of the stack. This was eliminated by warming the flange with electrical heater tape.

## SECTION 6

## ELECTRONICS AND DATA ACQUISITION

The electrical schematic for the complete monitor system is shown in Figure 16. A photograph of the portable electronics cases is given in Figure 17. In the photograph, the case to the left contains the laser control modules, LCM, and the lock loop amplifiers, PSD. Also contained in this case is an oscilloscope used to view the infrared detector outputs during alignment and line locking of the lasers. Above the case are the two cryogenic temperature stabilizers, CTS. In field operation, these units must be located in close proximity to the optical pallet whereas the two cases may be remotely positioned.

The case to the right in Figure 17 contains the data acquisition system. This consists of four lock-in amplifiers, PSD, which are coupled to the calculator through the analog to digital converter, ADC. The calculator is out of view inside the drawer at the top of the case. Specific details of the interconnections are given in the Systems Operations Manual.

Data acquisition is controlled by a Hewlett Packard 9815S calculator. A description of the software and a program listing are given in the Systems Operations Manual.

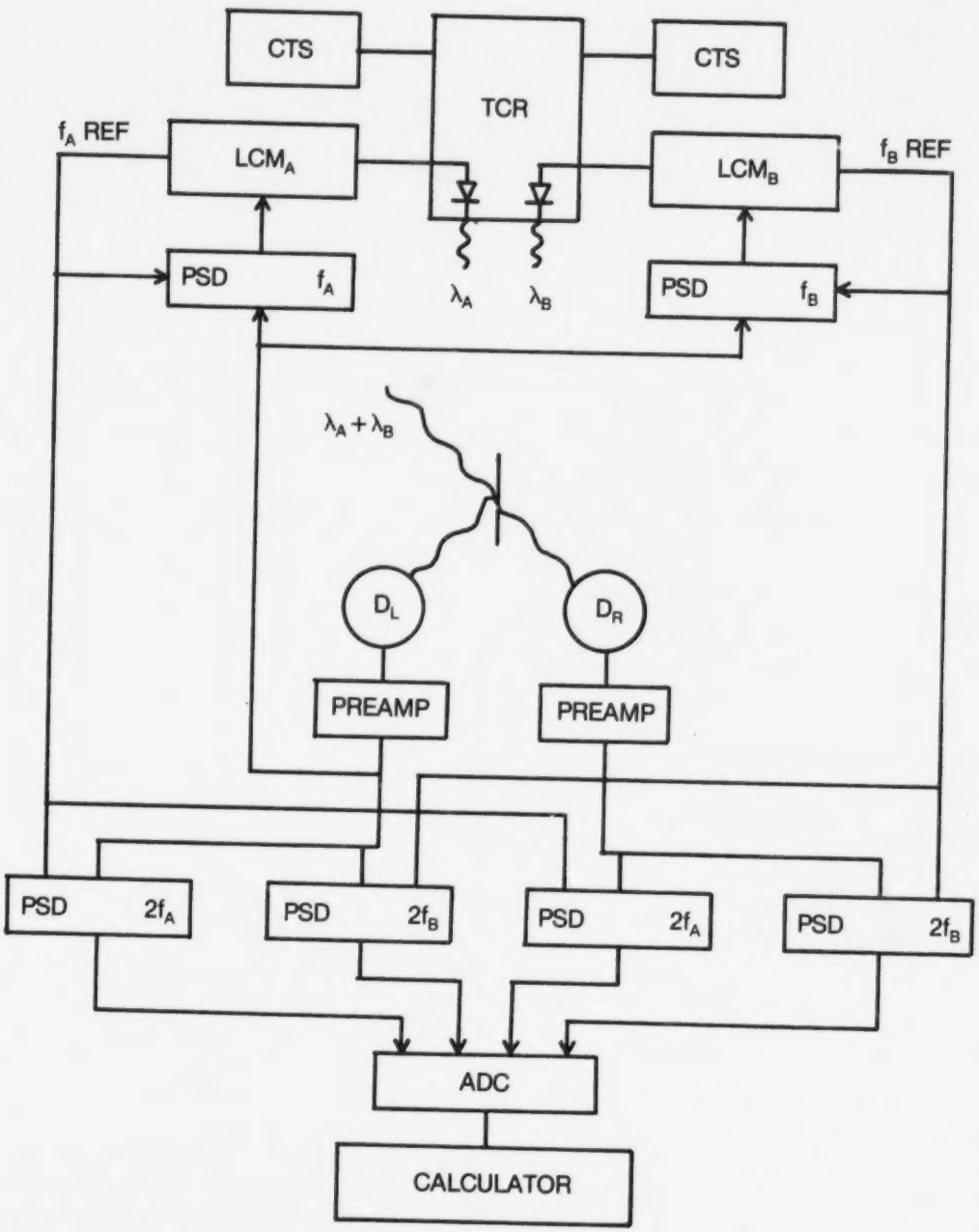


Figure 16. Laser control and data acquisition system block diagram.

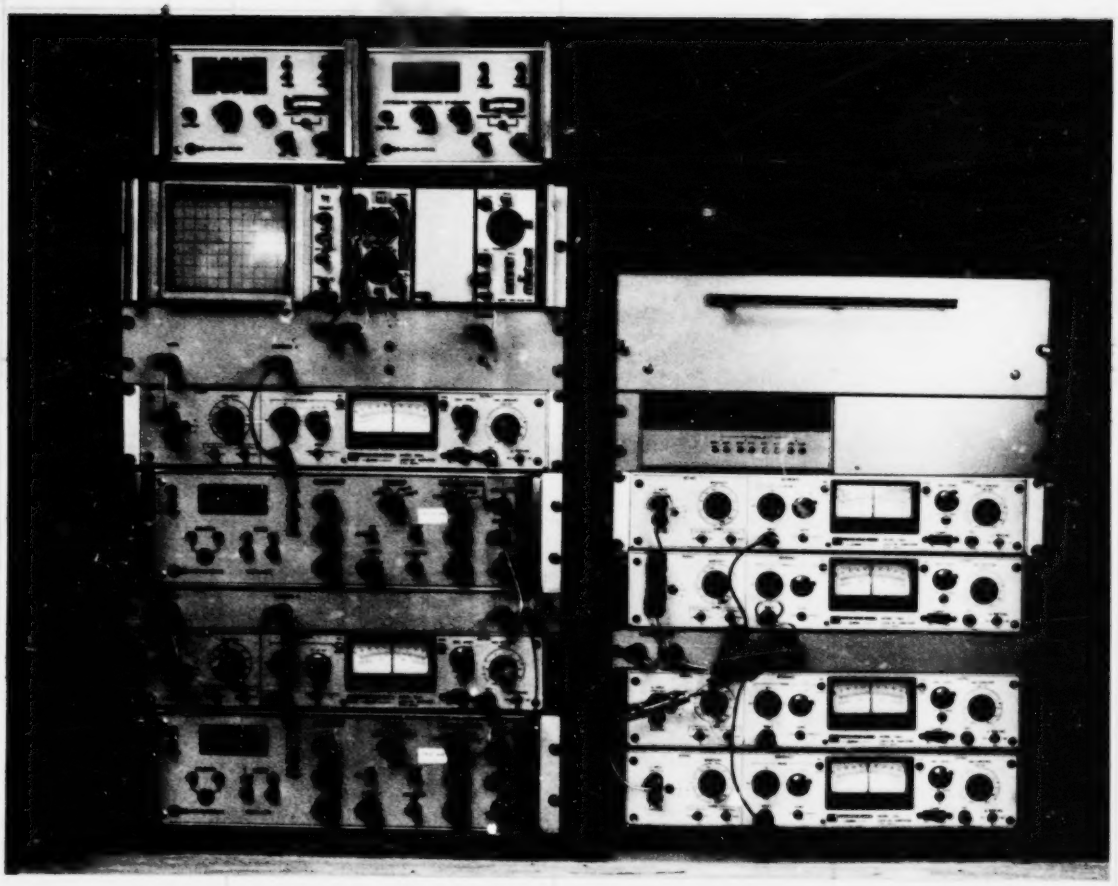

Figure 17. Photograph of electronics and data acquisition system.

## SECTION 7

## $H_2SO_4$ CALIBRATION CELL

### DESIGN CONSIDERATIONS

The apparatus described in this section is designed for laboratory calibration of the monitor instrument. It attaches directly to the optical pallet of the monitor. Measurements are conducted in the same manner as cross stack measurements.

The absorption cell and its copper heat shield are shown in Figure 18. The cell is constructed of one inch diameter pyrex tubing with an overall length of 14 inches. Two silicon windows are fused into the pyrex tubing with an 8 inch absorption path between them. The fused windows provide a rugged vacuum seal which can withstand thermal cycling and high temperature $H_2SO_4$ vapor without deterioration. To maintain uniform temperature over the absorption path, the 12 inch long heating jacket extends beyond the silicon windows. The cell body extends three inches beyond each silicon window, and the ends of the tube are closed with $BaF_2$ windows which serve to prevent cool air circulation to the silicon windows to the cell. To prevent etalon problems all windows are installed about three degrees off from normal incidence to the optical path. A 50 ml reservoir bulb contains the liquid sample. The cell, reservoir and connecting neck are separately heated. To maintain uniformity over the absorption path, the cell is surrounded by a copper jacket 12 inches long. A cylindrical heating mantle is fitted over the copper jacket. Reservoir temperature is controlled by a standard spherical heating mantle. To insure that no cold spots occurred in the connecting neck, this region was wrapped with a heating tape. Both of the heating mantles are regulated by current proportional temperature controllers which have an accuracy of ±0.1C. A variable autotransformer controls the neck heater. Ten thermocouple sensors are located on the cell and copper jacket. Their positions are indicated in Figure 18. Temperature readout is provided by a digital thermometer with a resolution of 0.2°C.

The optical pallet containing the calibration cell is shown in Figure 19. Figure 20 is a photograph of the cell attached to the monitor. Also shown is the control cabinet containing the proportional controls and the digital thermometer. The cell is supported by the cylindrical heating mantle which is cradled in adjustable supports that permit optical alignment. The reservoir bulb is suspended freely below the pallet. This arrangement is very stable and shows no noticeable displacement of the cell through thermal cycling.

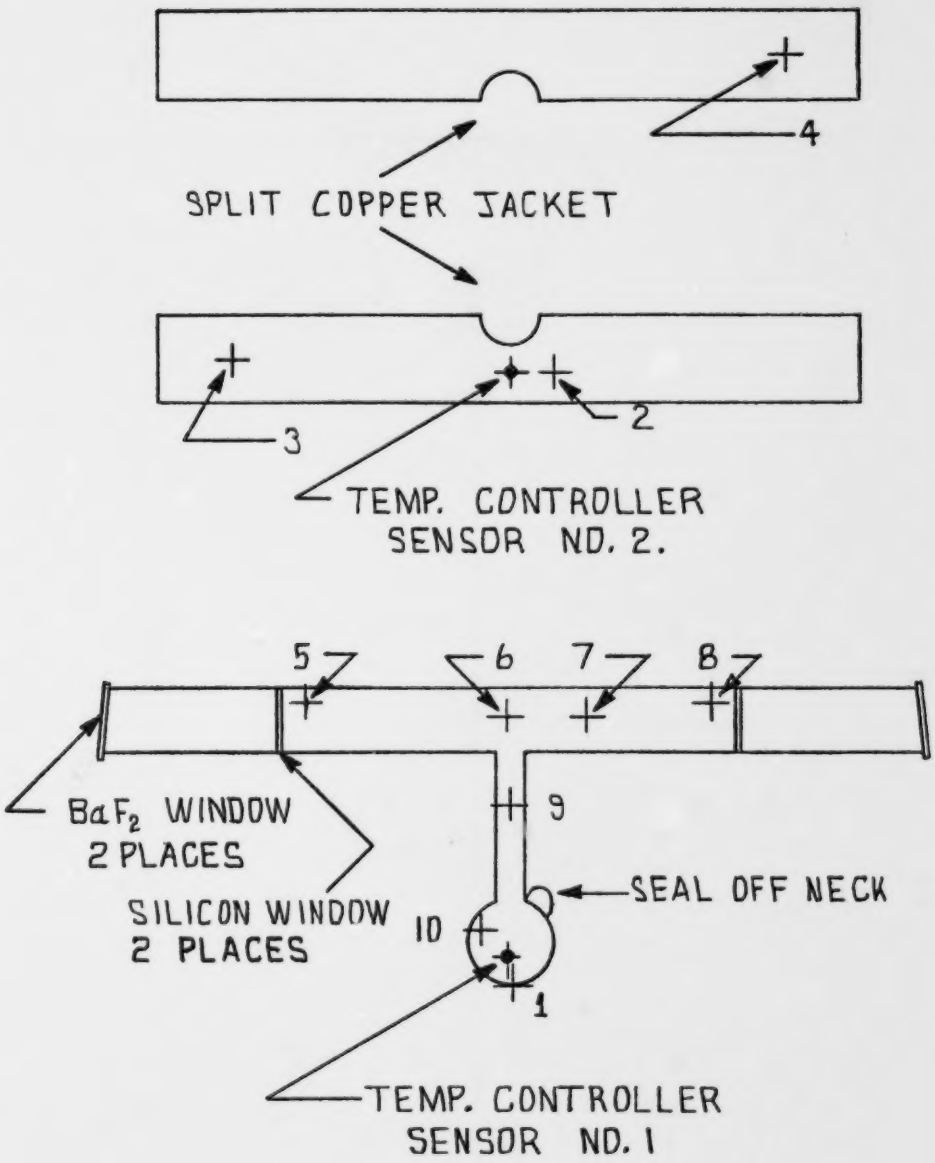


Figure 18. $H_2SO_4$ calibration cell diagram showing liquid azeotrope reservoir, absorption path and copper heating jacket.

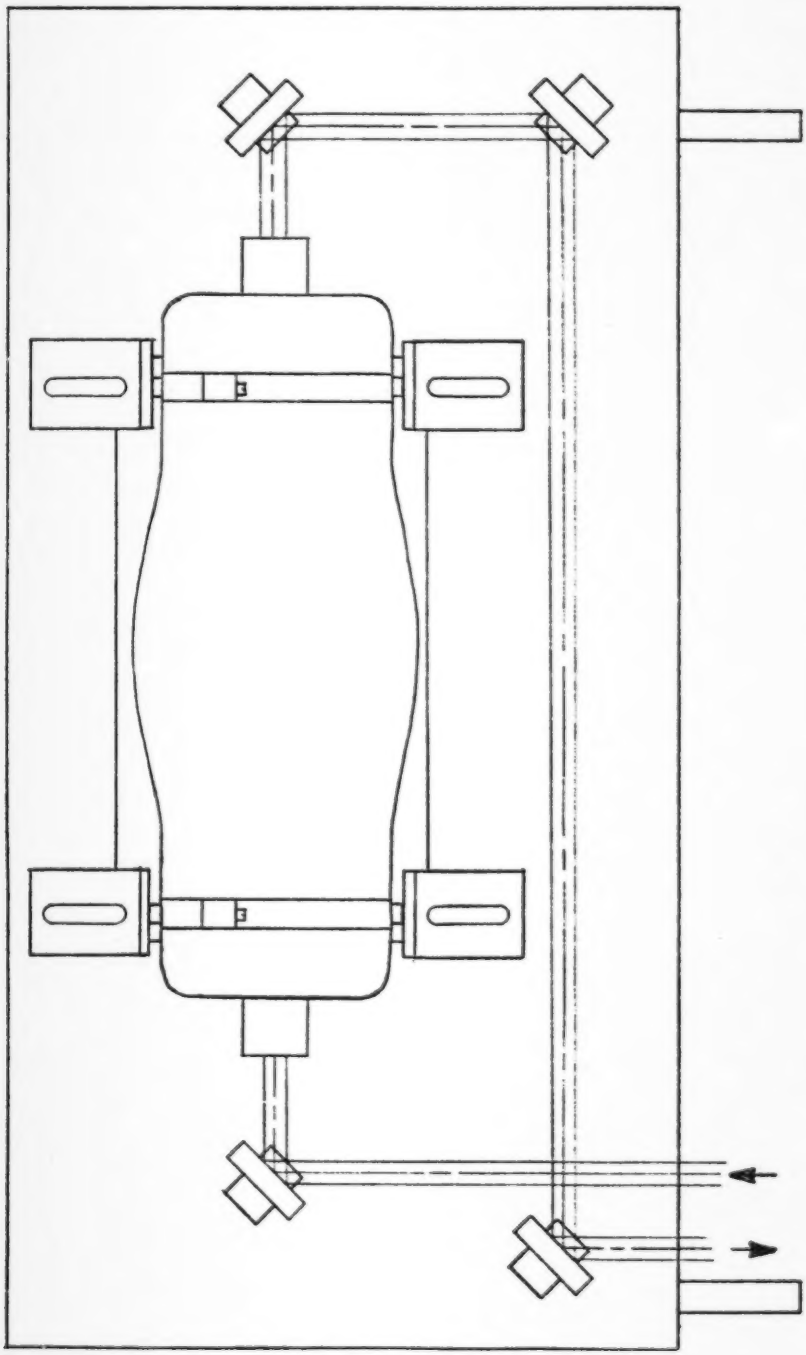

Figure 19. $H_2SO_4$ calibration cell pallet optical diagram.

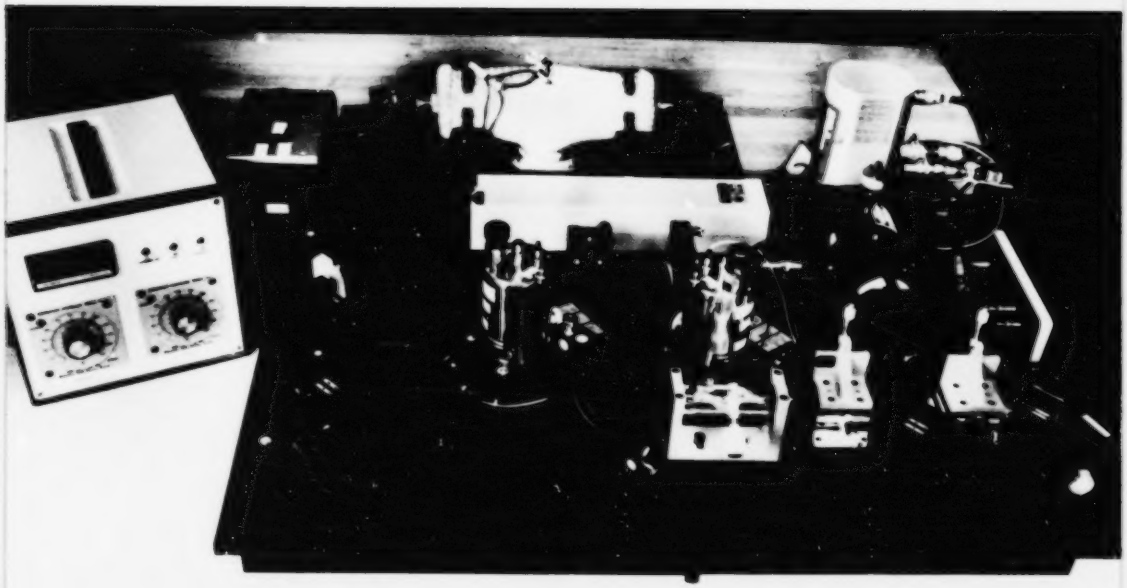

Figure 20. Photograph of $H_2SO_4$ calibration cell attached to monitor optical pallet.

Preparation of the cell began by filling the reservoir 2/3 full with a 37 normal $H_2SO_4$ solution. The cell was evacuated and heated to 180°C. An azeotropic mixture was obtained by distilling away about 1/3 of the liquid before the cell was cooled. The first cell prepared was backfilled with dry nitrogen before it was sealed. This atmospheric pressure version proved to be unworkable because the partial pressure of $H_2SO_4$ could not equilibrate between the cell and the reservoir. An evacuated cell was adopted when it was demonstrated that an equilibrium could be achieved in this manner. The sealed cell was tested with a tesla coil to verify that a good vacuum had been preserved.

## CALIBRATION MEASUREMENTS

The calibration cell pallet was first aligned to the monitor with the cell removed. The cell was then installed and positioned to give maximum transmitted signal. Insertion loss for the cool cell approached 90 percent. This loss comes primarily from the silicon windows.

Optical normalization was determined for the cell at room temperature. The cell mantle was switched on and the cell was allowed to stabilize at a set temperature. The change in differential window absorption was recorded. The reservoir was then heated and allowed to stabilize at a temperature below that of the cell or neck. Measurements were recorded only after the differential absorbance was observed to vary by less than 0.01 units over a period greater than ten minutes. Results of six measurement runs are given in Table 3.

TABLE 3. CALIBRATION CELL MEASUREMENT RESULTS

| Run No. | $T_{bulb}$ °C | $T_{cell}$ | Absorbance | $P_{H_2SO_4}$ (Torr) | $S_A - S_B$ (ppm-$m^{-1}$x$10^4$) |
|---|---|---|---|---|---|
| 1 | 200 | 206 | 1.15 | 4.17 | 10.3 |
| 2 | 188 | 206 | 0.49 | 2.12 | 8.7 |
| 3 | 190 | 192 | 0.98 | 2.90 | 12.6 |
| 4 | 185 | 192 | 0.81 | 2.20 | 13.8 |
| 5 | 169 | 192 | 0.34 | 0.83 | 15.1 |
| 6 | 180 | 192 | 0.56 | 1.64 | 12.8 |

The absorbance column in Table 3 gives the net differential absorbance due to the $H_2SO_4$ vapor. Partial pressures given for $H_2SO_4$ are taken from Lutschinski [9]. They have been corrected to account for dissociation in going from the reservoir bulb to the hotter cell. The results given in the last column are differential absorption coefficients per unit $H_2SO_4$ vapor concentration. From the work of Burch et al.[1] the absorption coefficient in the 962 $cm^{-1}$ background region ($S_B$) can be estimated to be .09 of the peak absorption coefficient ($S_A$) in the 880 $cm^{-1}$ band. Taking an average value of

$S_A - S_B = 12.2 \pm 2.3 \times 10^{-4}$ $ppm^{-1}m^{-1}$ the peak absorption coefficient, $S_A$, for the band is $13.3 \times 10^{-4}$ $ppm^{-1}m^{-1}$. This is a substantial increase over the value of $7.0 \times 10^{-4}$ $ppm^{-1}m^{-1}$ reported by Eng and co-workers[3].

A closed form analytical model incorporating temperature dependent parameters has been formulated in order to better understand the $H_2SO_4$ liquid-vapor system. Partial pressures above the $H_2SO_4$ azeotrope at temperature T are given by (from Lutschinski) (9).

$$P_{H_2O}(T) = 10^{[9.603-4423/T]} \tag{1}$$

$$P_{SO_3}(T) = 10^{[10.1475-4748/T]} \tag{2}$$

$$P_{H_2SO_4}(T) = 10^{[9.059-3976/T]} \tag{3}$$

$$P_{Total}(T) = P_{H_2SO_4}(T) + P_{H_2O}(T) + P_{SO_3}(T) \tag{4}$$

In our case the azeotrope is maintained at a temperature $T_R$ and the absorption path is maintained at temperature $T_C$ where $T_C \geq T_R$.

For the sulfuric acid azeotrope the temperature dependent equilibrium dissociation constant, K, (T), is given by

$$K(T) = \frac{P_{H_2O}(T)\ P_{SO_3}(T)}{P_{H_2SO_4}(T)} \quad . \tag{5}$$

So the equilibrium dissociation constants for the two temperatures $T_C$ and $T_R$ can be calculated in a straightforward manner from relations (1) through (4).

If we consider the volume immediately above the $H_2SO_4$ azeotrope solution to be in equilibrium, then

$$K(T_R) = \frac{P_{H_2O}(T_R)\ P_{SO_3}(T_R)}{P_{H_2SO_4}(T_R)} \tag{6}$$

In the absorption cell, at temperature $T_C$, we approximate the equilibrium dissociation constant by equation (7) where $\Delta P$ is a small change in pressure.

$$K(T_C) = \frac{P_{H_2O}(T_r) + \Delta P)\ (P_{SO_3}(T_R) + \Delta P)}{(P_{H_2SO_4}(T_R) - \Delta P)} \tag{7}$$

We can calculate $\Delta P$ from equation (7), and we calculate a final $H_2SO_4$ pressure in the cell body from the relation

$$P_{final}(H_2SO_4) = (P_{H_2SO_4}(T_R) - \Delta P) \frac{P_t}{P_t + \Delta P} \quad (8)$$

where $P_t/(P_t + \Delta P)$ is a small pressure correction and $P_{final}$ is the sulfuric acid pressure that contributes to the Beer's law absorption.

Figures 21 and 22 present the results of Table 3 along with absorbances calculated from the above relations for various assumed values of the absorption coefficient. Consistent results are seen in Figure 21 for a constant cell body temperature of 192°C. Lower values for the absorption coefficient, shown in Figure 22, were obtained when the cell was maintained at 206°C. This tends to suggest dissociation problems associated with hot spots. However, there are not sufficient grounds for rejecting this data. Therefore, our final value of the absorption coefficient is the average of the six measurements given above.

In reviewing the earlier work the following distinctions should be considered:

1. The absorption cell used in the present measurements was well controlled thermally. Temperatures of both the cell and the reservoir were regulated by current proportional controllers. Thermocouple sensors on the cell gave temperature profiles during each experimental run. The maximum variation noted was 2.7°C. In the earlier work only the reservoir was heated with a feedback controller. The cell body was warmed by electrical heating tape connected to a variable transformer. Temperature uniformity along the cell was not adequately confirmed. Hot or cold spots with variations 10°C or greater cannot be excluded.

2. Present measurements include smaller temperature separations between cell and reservoir than previously attempted. In the limit of very small differences the effects of further dissociation should disappear. The present study shows very good agreement between measurements at small and large temperature separations. This confirms that extra dissociation effects have been adequately treated.

3. Concern for aerosol generation led to the inclusion of a glass wool plug in the previous work. The present system has an unobstructed neck connecting the reservoir to the cell body.

4. A narrow neck side arm contained the liquid sample in the earlier measurement. In the present work the sample is contained in a bulb reservoir which provides a large area liquid-vapor interface. This affords greater confidence that the liquid and vapor are in equilibrium.

5. The $H_2SO_4$ monitor instrument used to make the present absorption coefficient measurements offers the considerable advantage of real time, con-

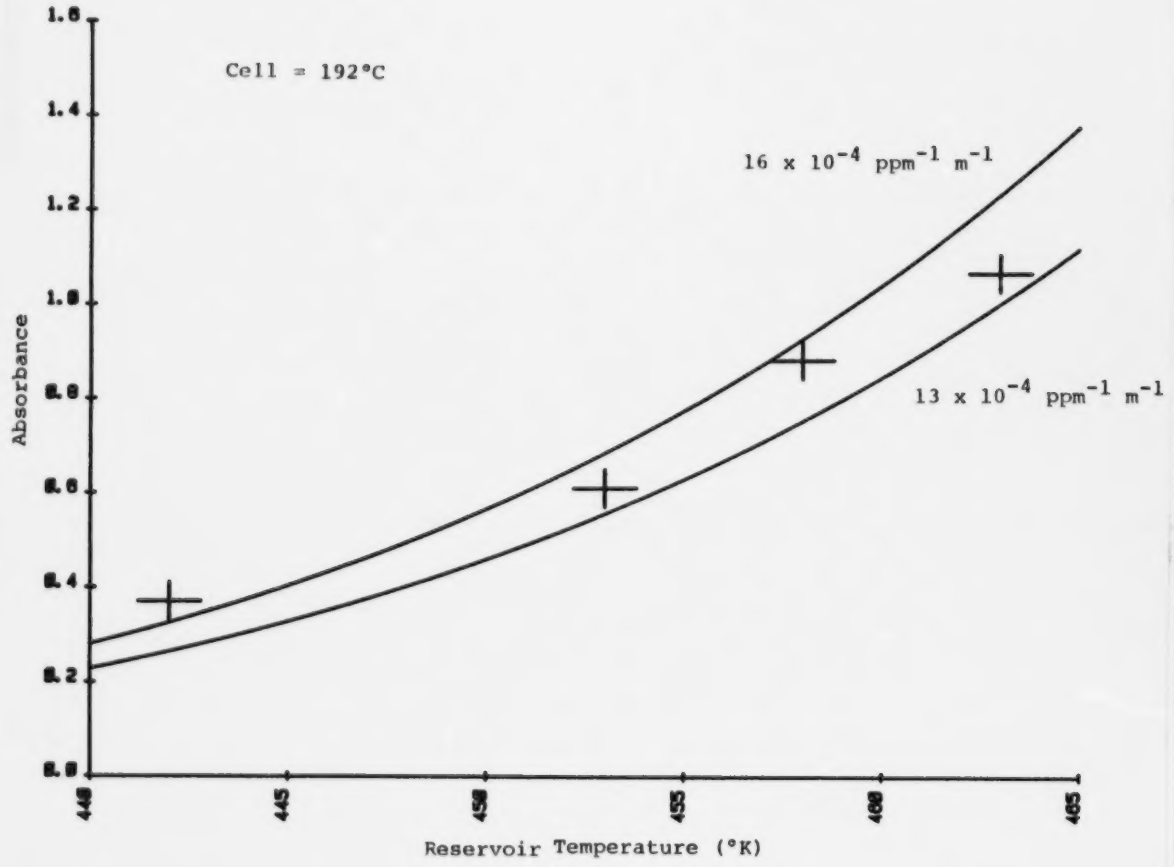


Figure 21. Calculated and measured absorbances of calibration cell as a function of reservoir temperature. Cell temperature 192°C.

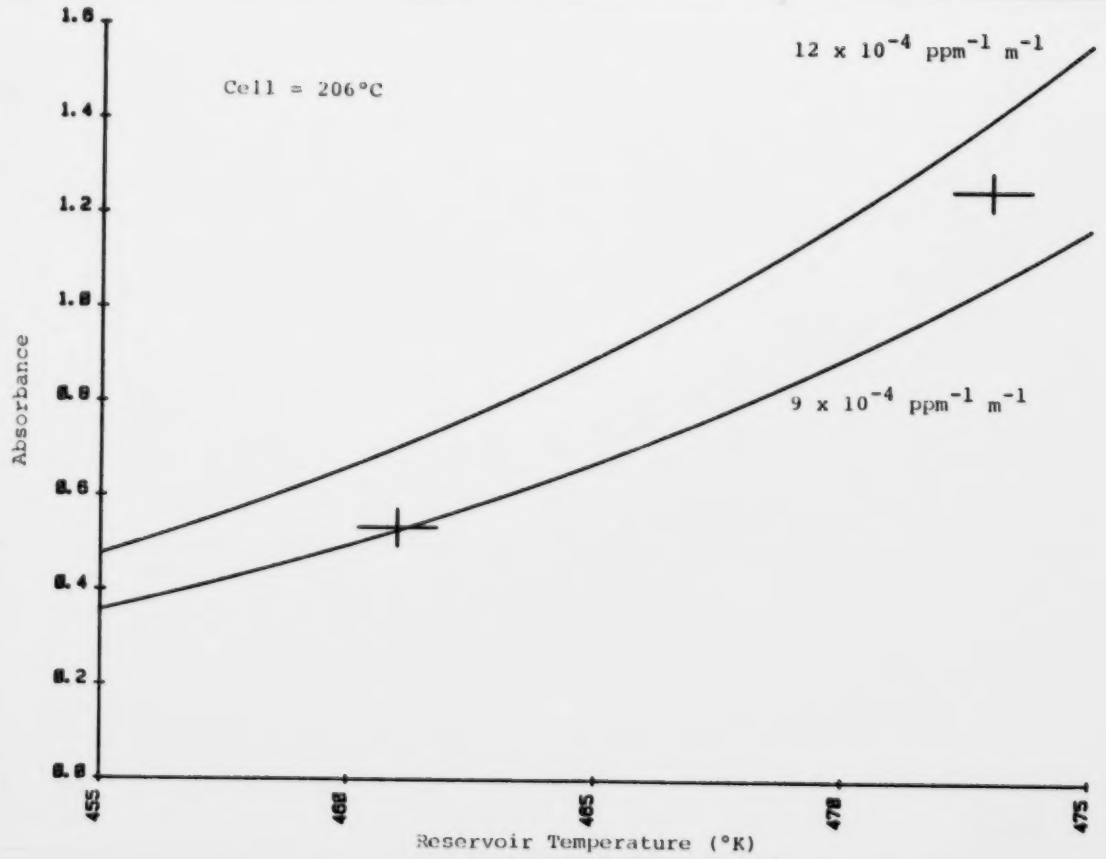


Figure 22. Calculated and measured absorbances of calibration cell as a function of reservoir temperature. Cell temperature 206°C.

tinuous measurement of the absorption cell. This permits accurate determination of stable conditions in the heated cell. Calibration measurements were accepted only after the vapor absorption remained stable for a period of from 10 to 40 minutes.

6. Partial pressures for the vapor above the $H_2SO_4$ azeotrope used in the present measurements were taken from Lutschenski[9]. Eng and co-workers (3) obtained independent results which are in good agreement with these values.

7. The present measurement is based upon a new modulation technique which is sensitive to the second harmonic of the laser modulation frequency. The earlier work was a conventional approach employing a beam chopping modulator and a single detector. For the second harmonic (second derivative) technique to yield a different result it is necessary to show that it offers a nonlinear response. Intensity measurements on carbon monoxide made at Laser Analytics, Inc. have shown that the method is indeed linear over the range of absorbance encountered in the $H_2SO_4$ measurements. We therefore are confident that the modulation and detection methods employed in this work do not introduce systematic errors into our results.

A reanalysis of the low pressure data taken by Eng and co-workers[3] has suggested that average cell temperatures were much higher than originally assumed. In this earlier work cell temperatures were taken to be close to the values measured at the windows. However a calculated dissociation constant $K_p(T)$ derived from comparisons of measurements with different reservoir temperatures but constant cell conditions implies a cell temperature of 228°C as opposed to the value of 200°C stated in the report. Such a temperature difference would increase the reported value of $7.0 \times 10^{-4}$ $ppm^{-1}$ $m^{-1}$.

In reviewing the earlier atmospheric pressure measurement (3) with the authors a possible cold spot was noted in the neck connecting the reservoir to the cell. This decrease in the effective reservoir temperature could have been as large as 6°C. In this case the measured absorption coefficient would be raised to $13 \times 10^{-4}$ $ppm^{-1}m^{-1}$.

Majkowski and co-workers[5] have reported a peak absorption coefficient of $17 \times 10^{-4}$ $ppm^{-1}m^{-1}$ for $H_2SO_4$ band at 1220 $cm^{-1}$. From the work of Burch and co-workers[1] it appears that this band and the 880 $cm^{-1}$ band have nearly equal peak strengths. It must be noted that the present results on the 880 $cm^{-1}$ band are low pressure measurements whereas results for the 1220 $cm^{-1}$ band were obtained in a flowing stream of nitrogen at atmospheric pressure. Nevertheless, for the broad $H_2SO_4$ bands considered the pressure broadening effects at one atmosphere can not introduce large changes in peak absorption. Majkowski[2] previously reported the much smaller value of $4.16 \times 10^{-4}$ $ppm^{-1}$ $m^{-1}$ for the 1220 $cm^{-1}$band. The jump in the value of the remeasurement was attributed to the elimination of hot spots and inclusion of excess dissociation corrections.

# SECTION 8

# FIELD TEST

## SITE SELECTION

A requirement of this program was that a field test be conducted at an electrical power generation plant burning high sulfur residual oil of Venezuelan origin. Such fuels, which are characterized by a high vanadium content, are used extensively in utilities in the eastern United States. The presence of heavy metals in the fuel is thought to increase sulfate generation through catalytic oxidation of sulfur dioxide.

The test site selected is one of the larger electrical generation plants in the northeastern United States. At the time of a site inspection in June, the test unit was undergoing periodic maintenance which permitted the installation of a slotted pipe in the duct near the entry to the stack. The 650 MW unit is operated as a base load unit running continuously at or near full output capacity. Fuels from 2-3 percent sulfur content are used, except for periods when local air quality levels prohibit the use of high sulfur content oil. Experimental areas consisted of 4 x 8 foot iron platforms on either side of the duct. These platforms were about 80 feet above ground and were accessible via ladders from a catwalk which crossed the top of the duct. Arrangements were made to shelter the electronics in a "covered bridge" section of the overhead catwalk and to have riggers raise all equipment directly from the ground to the platform and catwalk.

## TEST PLAN

To ensure adequate time for installation, alignment, and measurement, the following test plan was prepared.

| | |
|---|---|
| September 28 | Installation and protection of equipment. |
| September 29 | Prealignment. |
| September 30 | Contingency repair. |
| October 1 | Completion of installation and alignment. |
| October 2 | Measurements at normal operating conditions. |
| October 3 | Measurements during excess air increase program. |
| October 4 | Repeat of October 3's program. |
| October 5 | Removal of equipment. |

With a test area which was not protected from the weather, it was necessary to allow for time lost due to inclement conditions.

The original test date was set for the week August 17-24 with contingency plans for the following week. In the second week of August, the test unit suffered a boiler tube failure. Uncertainty in the repair schedule required postponement of the test until the first week of October.

## TEST CONDITIONS

All of the equipment was installed by riggers and LAI personnel on Friday, September 28. Plans to work over the weekend were aborted by a steady rain. Clear weather on Monday permitted completion of the installation and preliminary alignment. During visual alignment, condensation on the stack windows near the retroreflector was discovered. This was apparently the result of the combination of excess water leaking into the duct work and breezes cooling the flange. The flange near the optical pallet suffered no condensation problems probably because it was in a sheltered location and therefore remained warmer. Tuesday morning the condensation problem was eliminated by applying heating tape to the flange. Upon start up of the system a component failure was discovered in one of the LCM units. This was remedied by early afternoon. Sufficient time remained to conduct a startup test of the instrument and to make a short duration measurement across the stack.

The tests on October 3 proceeded on schedule until they were terminated by a severe thunderstorm with heavy rain at 15:40 hours. The unit operated at its normal level of 0.5 percent excess air until 10:30 when this was raised to 1.0 percent. At 14:20 an increase to 1.5 percent was made and maintained until local lightening activity forced a cessation of activity. Altogether, over 5 hours of observations were made.

On the morning of October 4, the test unit was found to be operating above 0.7 percent excess air. This situation could not be corrected until after 11:00 a.m. Two and one-half hours were required to reduce the excess air and allow the unit to stabilize at the normal level of 0.5 percent. The time lost ruled out the planned two-step air increase program. At 14:00 a single step from 0.5 to 1.5 percent was executed. Over a 12 hour period the monitor followed the $H_2SO_4$ production response to the increase and subsequent decrease in excess air.

Equipment removal was completed on October 5 just before a second rain began. In spite of wet weather conditions no part of the system suffered discernable damage in the course of the test.

Throughout all of the tests an electrostatic precipitator was in operation. A fuel additive containing MgO was supplied continuously and was not altered during excess air increase programs.

## RESULTS

Data collection on October 2 was limited because of the malfunction in the LCM. The first tests were stability checks. Maximum drift was .017 absorbance units over a 36 minute period. These tests were performed with a retroreflector located before the stack. Several alignment iterations were made to confirm the repeatability of the procedure. The first stack test commenced at 17:22 and lasted about 40 minutes. Results are shown in Figure 23. Although the software for the calculator permitted direct readout in $H_2SO_4$ vapor concentration, testing was conducted with data output in absorbance units. This permitted better understanding of the magnitude of system fluctuations and allowed evaluation of system response free from questions concerning the exact value of the absorption coefficient. Interpretation of the results also requires a measurement of the differential absorbance of the stack windows. Prior to the field test this was measured in the laboratory to be 0.36 $\pm$ .04 absorbance units. Following the field test the windows were re-evaluated in the laboratory. No change attributable to surface deposits could be determined. The uncertainty in the window differential absorption is primarily attributable to the fact that the surfaces of each window are not precisely parallel. This wedge cases small but detectable differences between visible (HeNe laser) and infrared alignments.

From the measurements on the laboratory calibration cell discussed in Section 7, the value of $12.2 \times 10^{-4}$ $ppm^{-1}$ $m^{-1}$ is taken for the net differential absorption, $(S_A-S_B)$, of $H_2SO_4$. Given the stack absorption pathlength of 5.5 m our results can be interpreted using a scale of 1.5 ppm per 0.01 absorbance units. The data in Figure 23 thus yields concentration ranging between 3 and 8 ppm.

October 3 measurements are presented in Figure 24. At 10:30 a.m., denoted as point a, the excess air was raised from 0.5 to 1.0 percent. This induced a rapid response followed by a steady rise until the excess air was stepped to 1.5 percent at 14:20; point b, on the plot. Less than 90 minutes of data were obtained at the peak air level before the rain terminated the run. All gaps in the plot represent periods during which the alignment and normalization were being checked by putting the shorting retroreflector in place. The large downward spike at c was caused by personnel stepping onto the platform to secure the instrument against the weather. Sulfuric acid concentration results range from a starting level of 8 ppm to a final, maximum concentration of 40 ppm.

Figure 25 is a plot of the excess air program recorded in the control room for Unit No. 3. The trace showing the lesser values applies to the section of the boiler which exhausted into the duct on which the test was conducted.

Figure 26 gives the results of 12 hours of monitoring on October 4. The corresponding excess air program is shown in Figure 27. The plot begins at 9:44 a.m. and initially reflects a reduction in excess air to bring the unit to a base level of 0.5 percent. Particular features and events indicated by the letters on the plot are identified as follows:

```
A-R  SENSITIVITY      TIME    HH.MM                -4.03 -01
       10.00 -03               5.22                -4.01 -01
                                                   -3.97 -01
B-R  SENSITIVITY                                   -4.02 -01
       25.00 -03      PRINT INTERVAL               -3.99 -01
                       (SECONDS)                   -3.98 -01
A-L  SENSITIVITY                30                 -3.96 -01
       10.00 -03              -4.12 -01           -3.96 -01
                              -4.11 -01           -3.97 -01
B-L  SENSITIVITY              -4.17 -01           -3.95 -01
       10.00 -03              -4.11 -01           -3.97 -01
                              -4.14 -01           -3.97 -01
                              -4.12 -01           -3.99 -01
A-R  OFFSET                   -4.11 -01           -3.99 -01
        0.00  00              -4.14 -01           -4.00 -01
                              -4.11 -01           -3.98 -01
B-R  OFFSET                   -4.12 -01           -3.95 -01
        0.00  00              -4.11 -01           -3.97 -01
                              -4.07 -01           -3.96 -01
A-L  OFFSET                   -4.07 -01           -3.92 -01
        0.00  00              -4.02 -01           -3.92 -01
                              -4.05 -01           -3.87 -01
B-L  OFFSET                   -4.02 -01           -3.91 -01
        0.00  00              -4.06 -01           -3.87 -01
                              -4.07 -01           -3.85 -01
                              -4.04 -01           -3.86 -01
                              -4.09 -01           -3.84 -01
NORM = 1.082  00              -4.01 -01           -3.85 -01
                              -4.06 -01           -3.82 -01
                              -4.04 -01           -3.80 -01
A-R  SENSITIVITY              -4.06 -01           -3.79 -01
        2.50 -03              -4.07 -01           -3.76 -01
                              -4.03 -01           -3.78 -01
B-R  SENSITIVITY              -4.05 -01           -3.77 -01
        2.50 -03              -4.05 -01           -3.77 -01
                              -4.04 -01           -3.75 -01
A-L  SENSITIVITY              -4.06 -01
       10.00 -03              -4.02 -01           -3.87 -01
                              -4.06 -01           -3.83 -01
B-L  SENSITIVITY              -4.01 -01
       10.00 -03              -4.01 -01
                              -4.04 -01
                              -3.99 -01           -3.82 -01
                              -4.04 -01           -3.82 -01
                              -4.00 -01           -3.86 -01
```

Figure 23. Calculator printout of measurements on Tuesday, October 2. Instrument sensitivity setting are given in the left column and test results are in the middle and right columns. Results given in absorbance units. ppm($H_2SO_4$) = 150 (a.u. - 0.36)

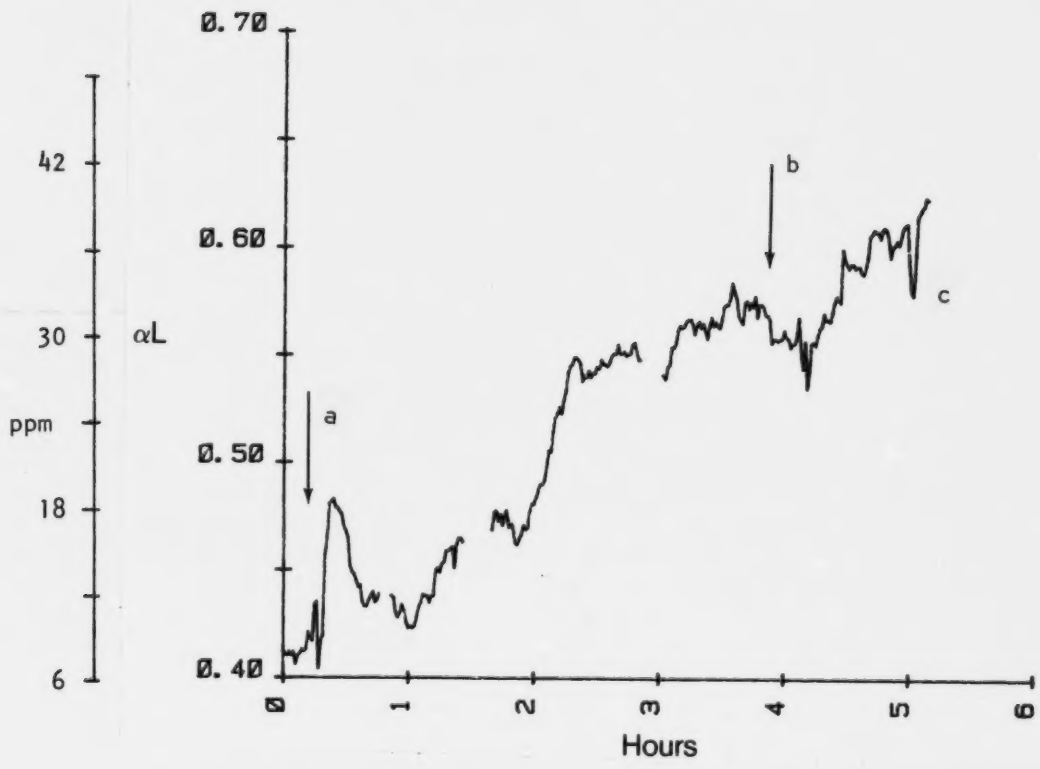


Figure 24. Measurement results for October 3. Arrows indicate excess air increases. Blank areas are periods when the monitor was in an internal test configuration. Time scale begins at 10:14 hours.

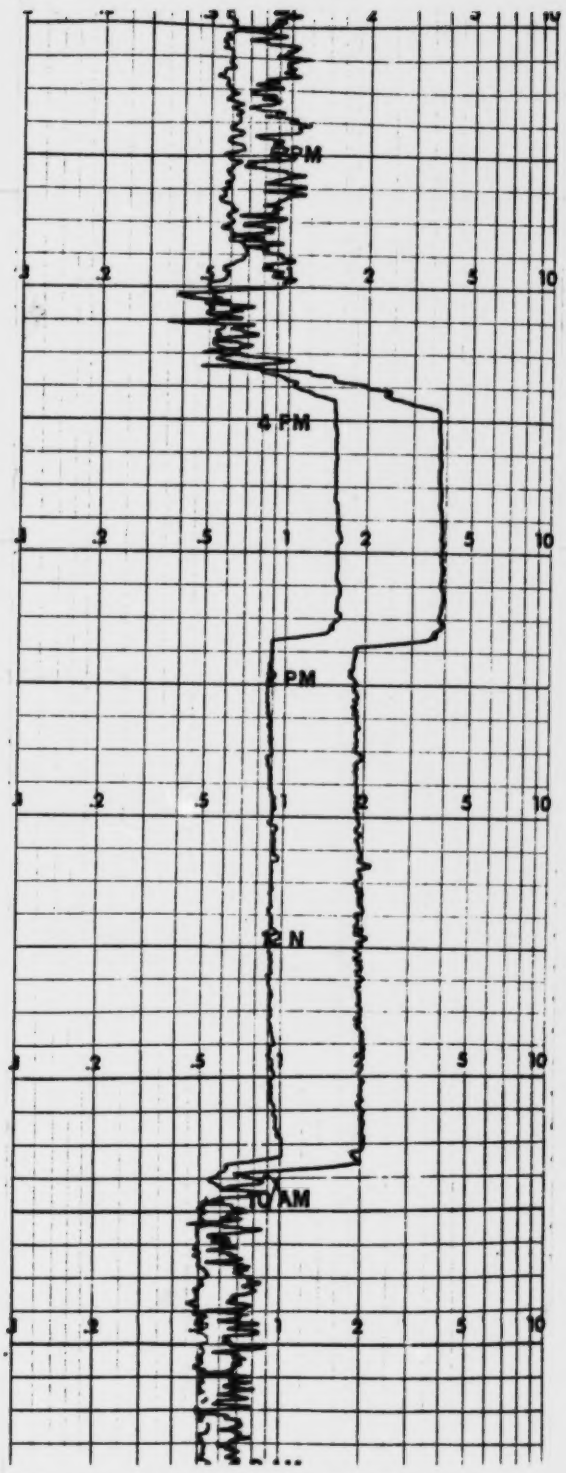


Figure 25. Control room record of excess air levels, October 3. Units are excess air in percent. Left trace applies to duct monitored.

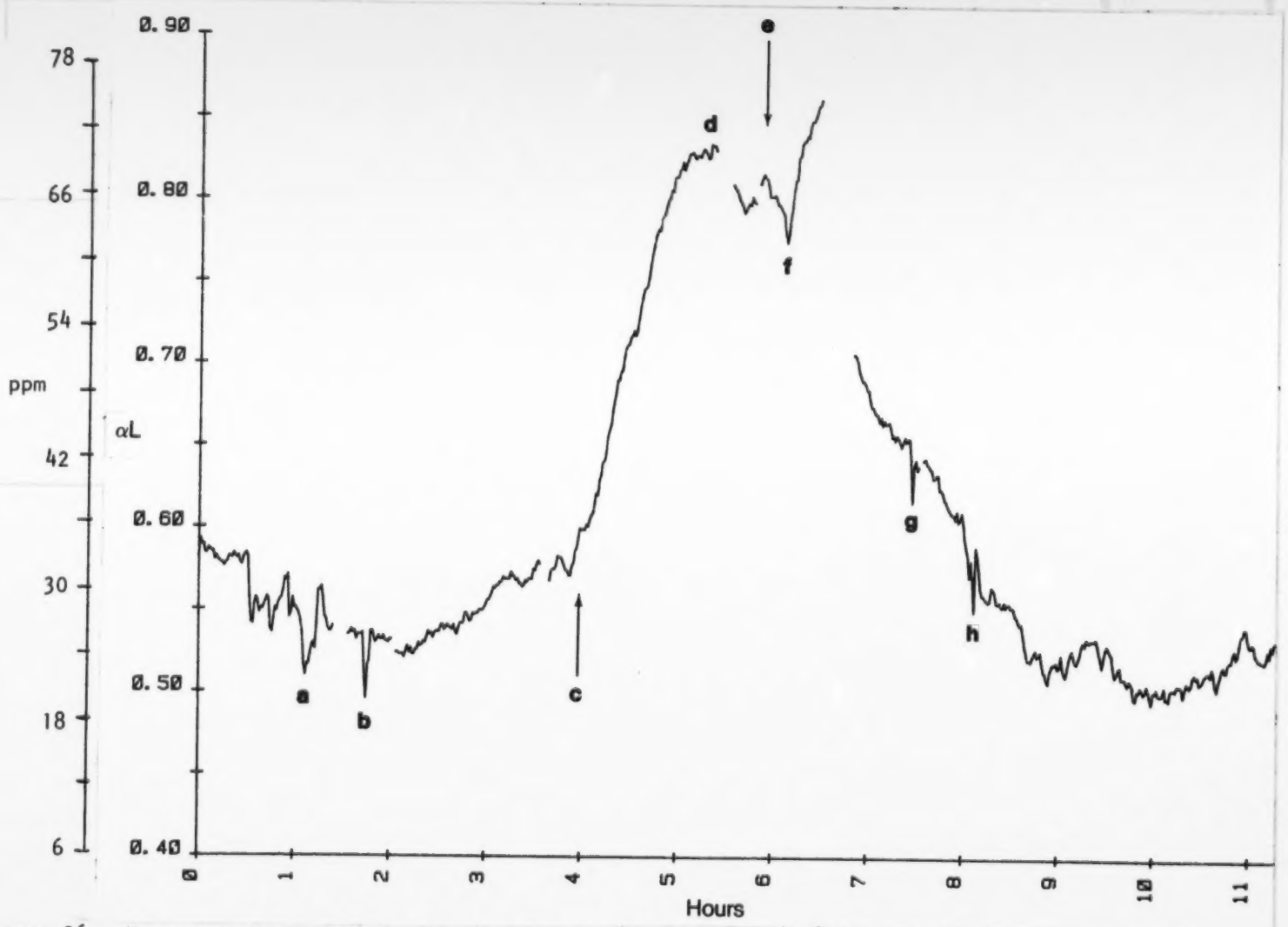


Figure 26. Measurement results for October 4. Arrows indicate excess air increase and decrease. Time scale begins at 09:44 hours.

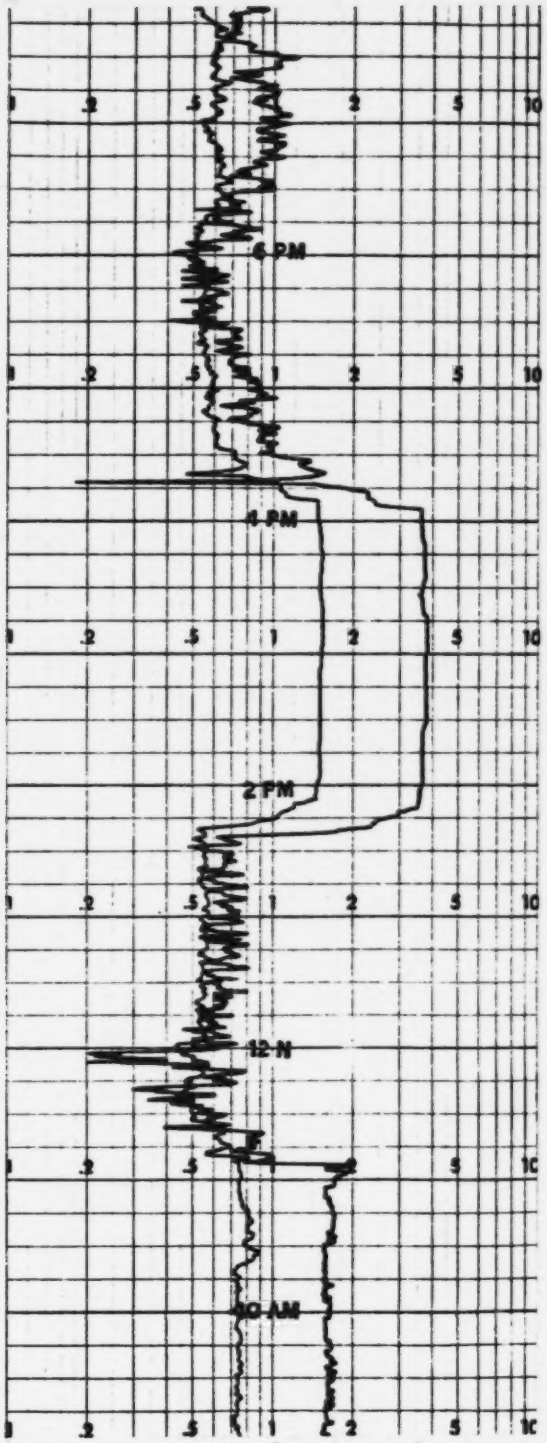


Figure 27. Control room record of excess air levels, October 4. Left trace applies to duct monitored. Units are excess air in percent.

a. Untility officials inspected the optical pallet platform.

b. Detectors replenished with coolant.

c. Excess air increased from 0.5 to 1.5 percent at 14:00.

d. Detectors replenished.

e. Excess air reduced to nominal level.

f. Excess air over corrected.

g. Visitors on platform.

h. Detectors replenished.

The lowest concentration recorded before the excess air was stepped upward was 25 ppm. Point d corresponding to 71 ppm was taken to be the best representation of the upper level. The resulting differential change, 71 - 25 = 46 ppm should be compared to the corresponding change of 32 ppm recorded the previous day.

The striking upward shift in the minimum $H_2SO_4$ level on October 4 (compared to that on October 3) is attributed to the greater than normal level of excess air encountered at the start of the day. Control room records reveal that the excess air had remained between 0.65 and 0.75 percent for over eight hours prior to the October 4 test program. The integrated effect of such a condition is to develop increased wall deposits on heat exchanger surfaces where catalytic oxidation of $SO_2$ occurs.

Careful checks of the optical alignment and system normalization showed that the monitor was functioning properly throughout the measurement period on October 4. There was no indication of any instrumental condition which would have given rise to a change in the minimum level.

## SUMMARY OF RESULTS

Measurements made on October 2 and 3 indicated base values of sulfuric and vapor concentration in the stack from 3 to 8 ppm. The minimum level of 25 ppm found on October 4 must be viewed in the perspective of the conditioning of the unit prior to the measurements. Measured changes of 32 and 46 ppm in acid vapor concentrations recorded October 3 and 4, respectively, represent consistent results for similar changes in combustion conditions. These measurements record the first continuous study of sulfuric acid concentrations in a stack. They demonstrated the feasibility of the dual wavelength differential absorption method to provide in situ, real time observations.

## REFERENCES


1. Burch, D. E., F. J. Gates, and N. Potter. Infrared Absorption by Sulfuric Acid Vapor. EPA-200/2-76-191, U.S. Environmental Protection Agency, Research Triangle Park, North Carolina, 1976. 27 pp.

2. Majkowski, R. F. Infrared Absorption Coefficient of $H_2SO_4$ Vapor From 1190 to 1260 $cm^{-1}$. J. Opt. Soc. Am., 67 (5): 624-627, 1977

3. Eng, R. S., K. W. Nill, and J. F. Butler, Spectral Measurements of Gaseous Sulfuric Acid Using Tunable Diode Lasers. EPA-600/2-78-019, U.S. Environmental Protection Agency, Research Triangle Park, North Carolina, 1978. 64 pp.

4. Eng, R. S., G. Petagna and K. W. Nill. Ultrahigh ($10^{-4}cm^{-1}$) Resolution Study of the 8.2-μm and 11.3-μm Bands of $H_2SO_4$: Accurate Determination of Absorbance and Dissociation Constants. Applied Optics, 17 (11): 1723-1726, 1978

5. Majkowski, R. F., R. J. Blint, and J. C. Hill. Infrared Absorption Coefficients of Gaseous $H_2SO_4$ and $SO_3$. Applied Optics, 17 (7): 975-977, 1978.

6. Mantz, A. W., Feasibility Measurements of Low Pressure Modulation Techniques for Frequency Selection. Laser Analytics, Inc., Internal Report, 1978.

7. Eng, R. S. A. W. Mantz, Investigation into Improved Sensitivity of Laser Absorption Techniques for Pollution Monitoring. National Science Foundation Grant ENV77-02124, Semiannual Report 2/1/79-8/1/79

8. Todd, T. R., Mantz, A. W., Final Report: Model LS-2X Laser Source Detector Test System, U.S. Army, CERCOM, Contract No. DAAB07-78-C-2465, 1979.

9. Lutschinski, G. P., Zh.Fig. Khim. 30:1207, 1956

# APPENDIX

## INTERFERENCE ABSORPTION SPECTRA

Figures A-1 through A-9 are plots of calculated interference absorptions from $H_2O$, $CO_2$ and $NO_2$ in the 880 and 960 $cm^{-1}$ regions. These plots are extensions of the calculated spectra given in Section 4. From an inspection of these figures it is clear that the number of spectral features resulting from these three stack gas components is non negligible. This illustrates the effectiveness of selective, high resolution minitoring techniques in minimizing sensitivity to stack gas interference as compared to techniques which integrate over several wavenumbers.

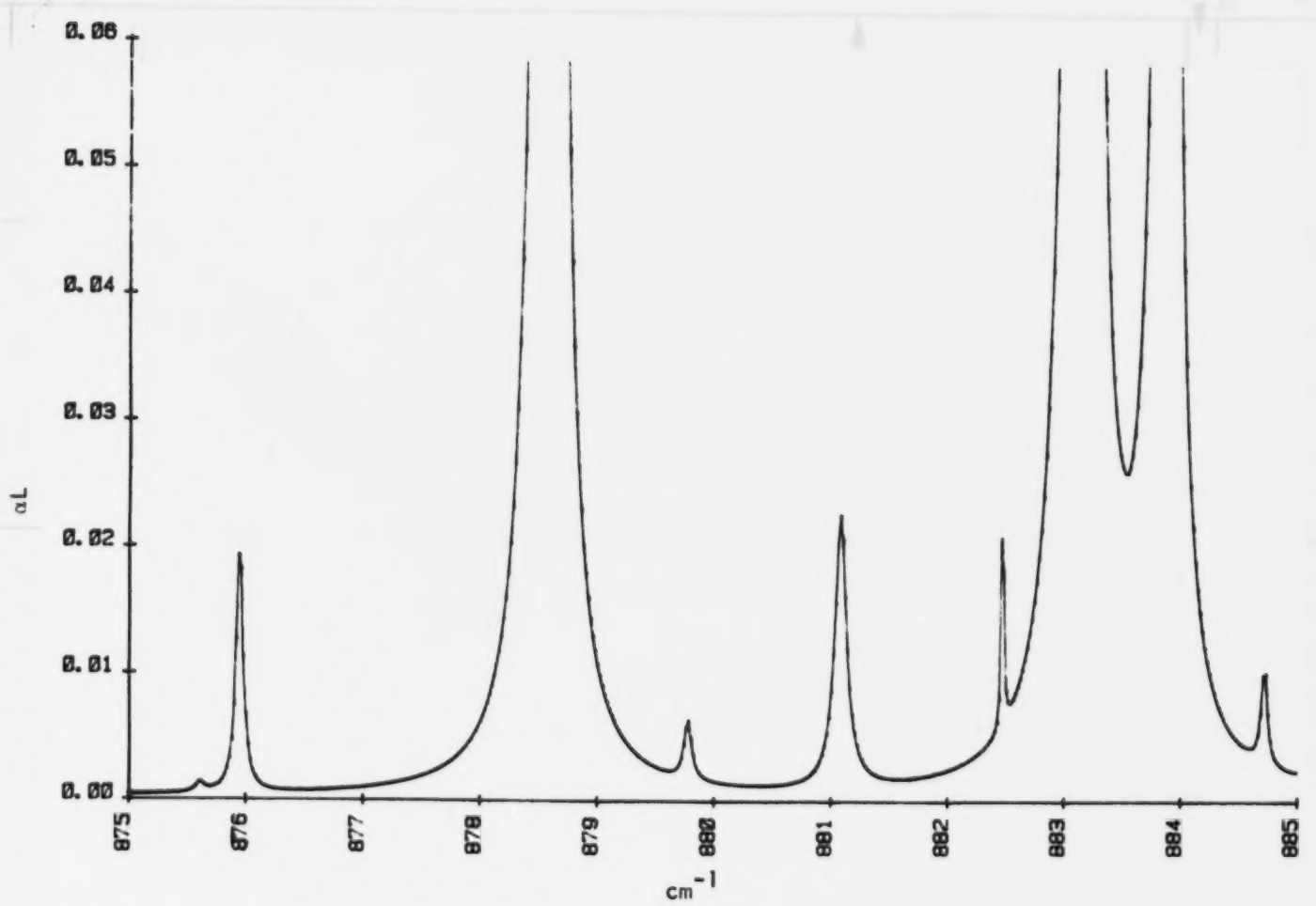


Figure A-1. Calculated $H_2O$ background absorption spectrum for 5 meter path at 473°K, 12% $H_2O$ (91 Torr) with data taken from the Air Force line listing in the 880 $cm^{-1}$ region.

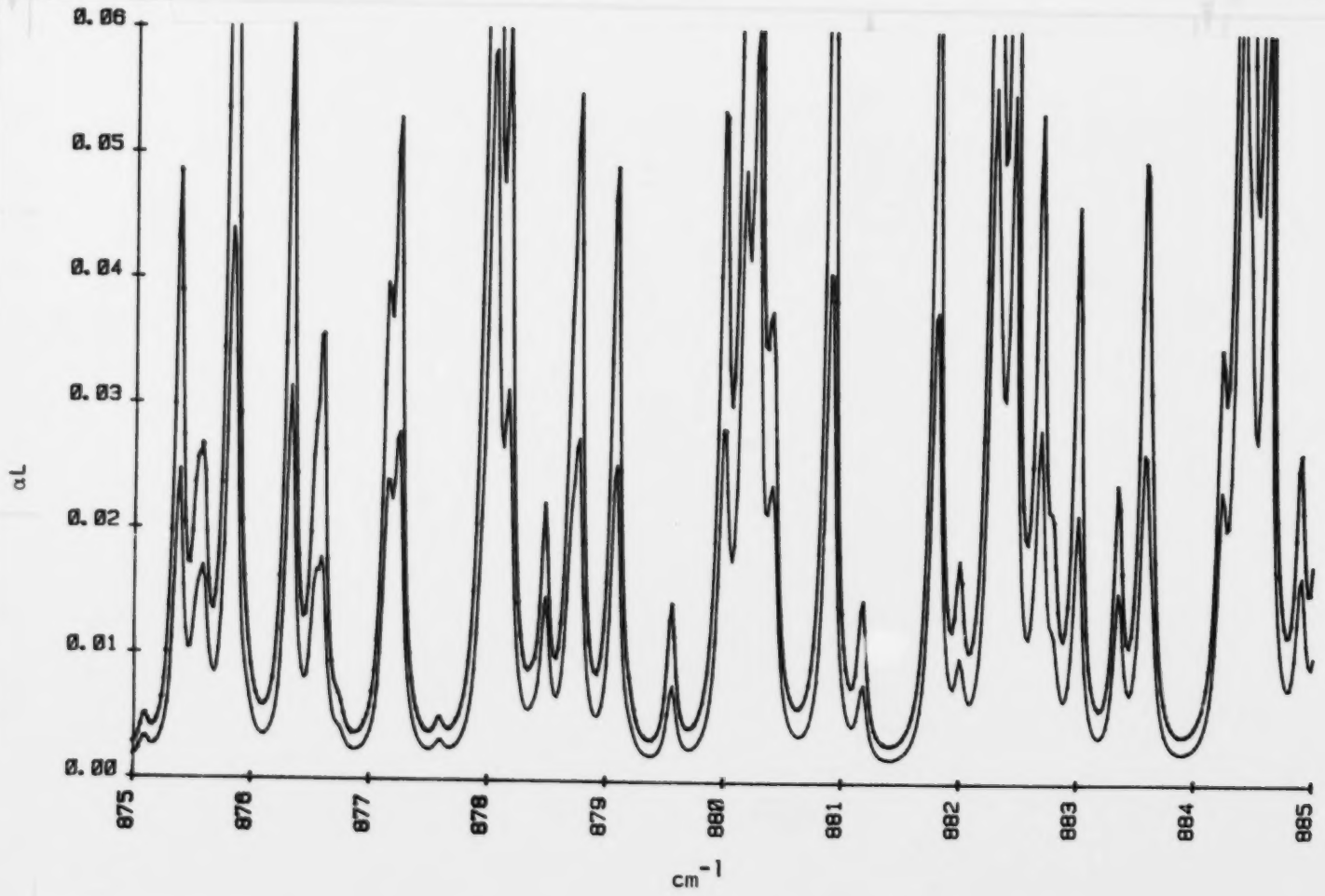


Figure A-2. Calculated $CO_2$ background absorption spectra for 5 meter path at 523°K and 473°K with a pressure of 114 Torr in the 880 $cm^{-1}$ region.

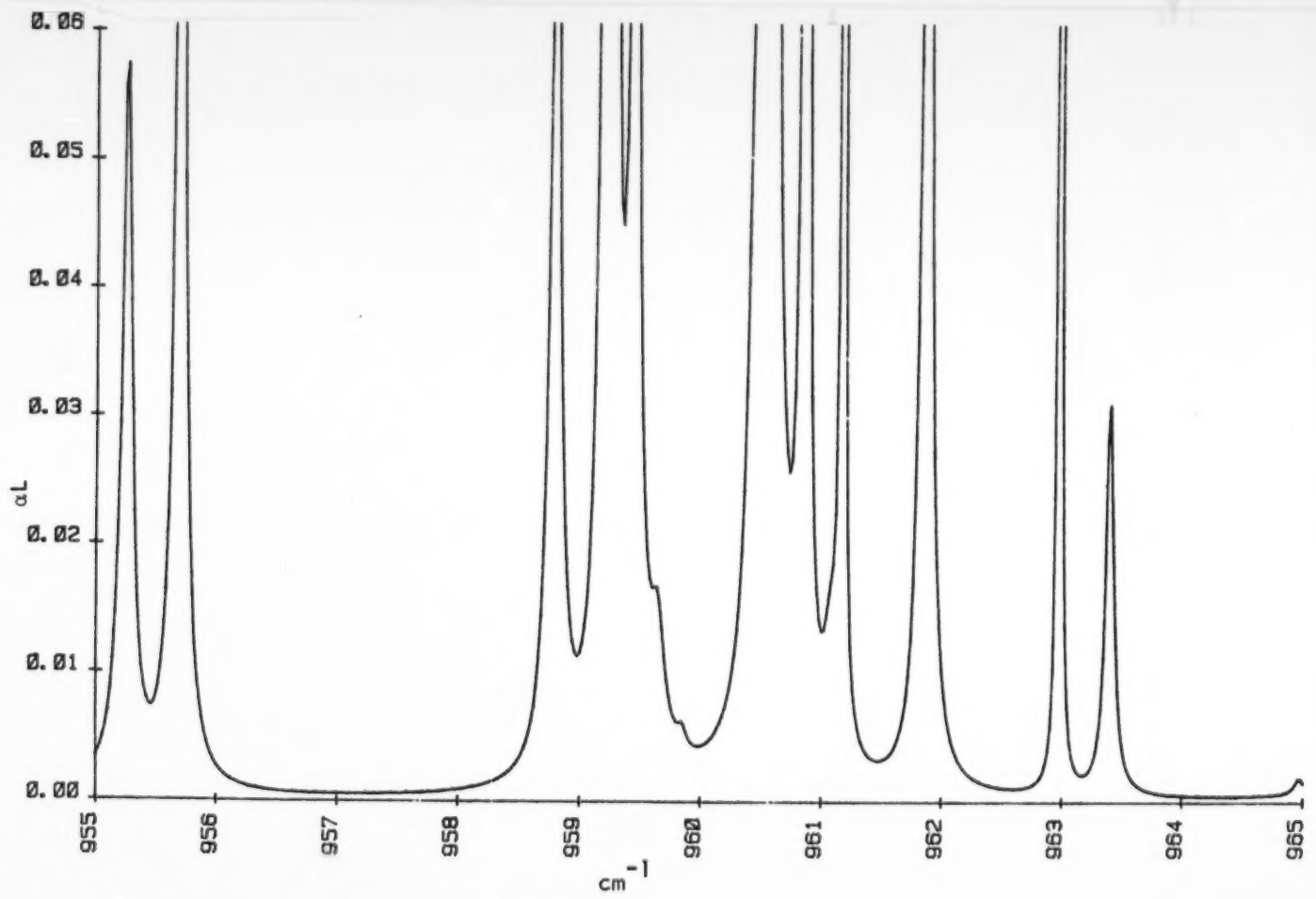


Figure A-3. Calculated $H_2O$ background absorption spectra for 5 meter path at 473°K, 91 Torr in the 960 $cm^{-1}$ region.

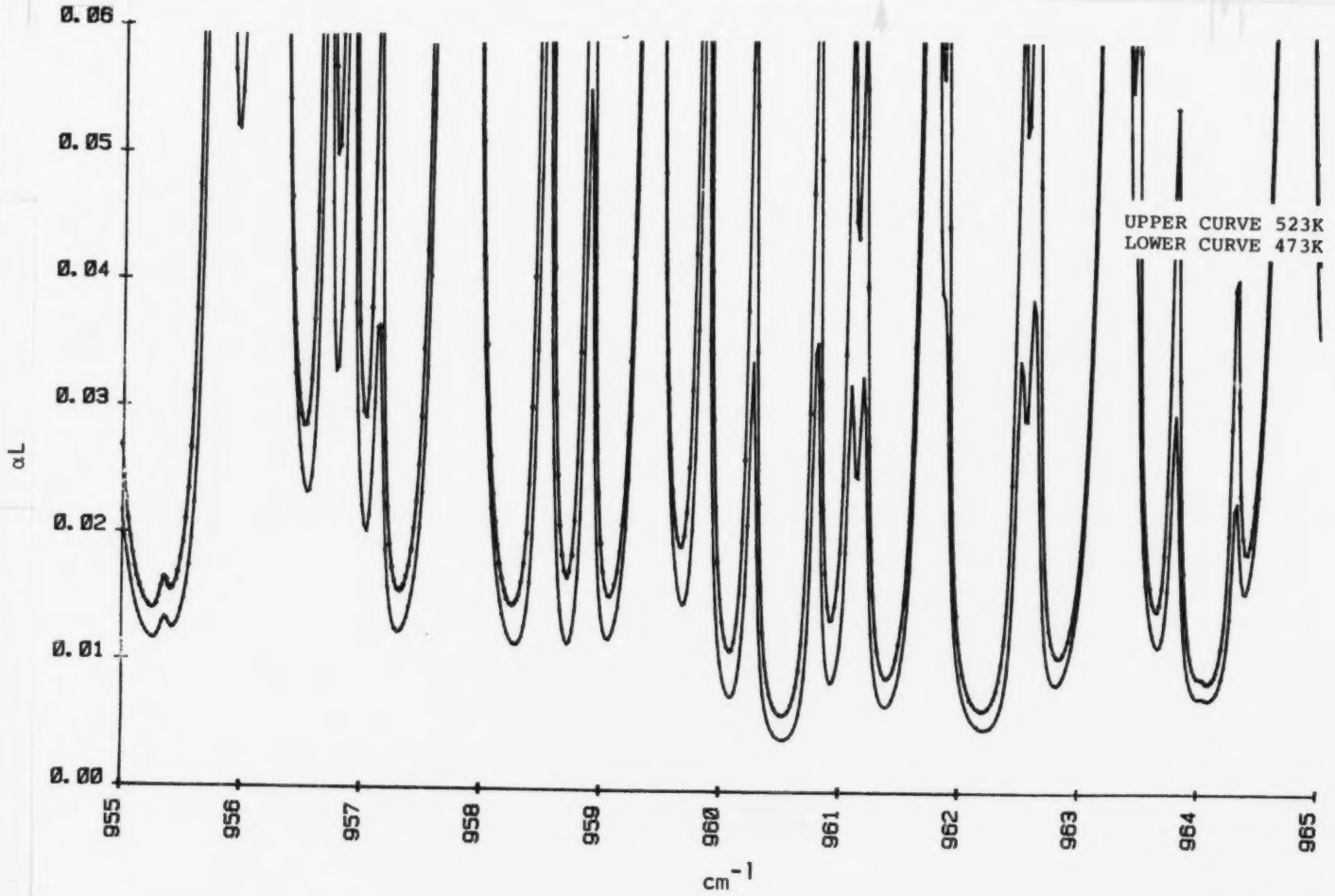


Figure A-4. Calculated $CO_2$ background absorption spectra for 5 meter path at 523°K and 473°K with a pressure of 114 Torr in the 960 $cm^{-1}$ region.

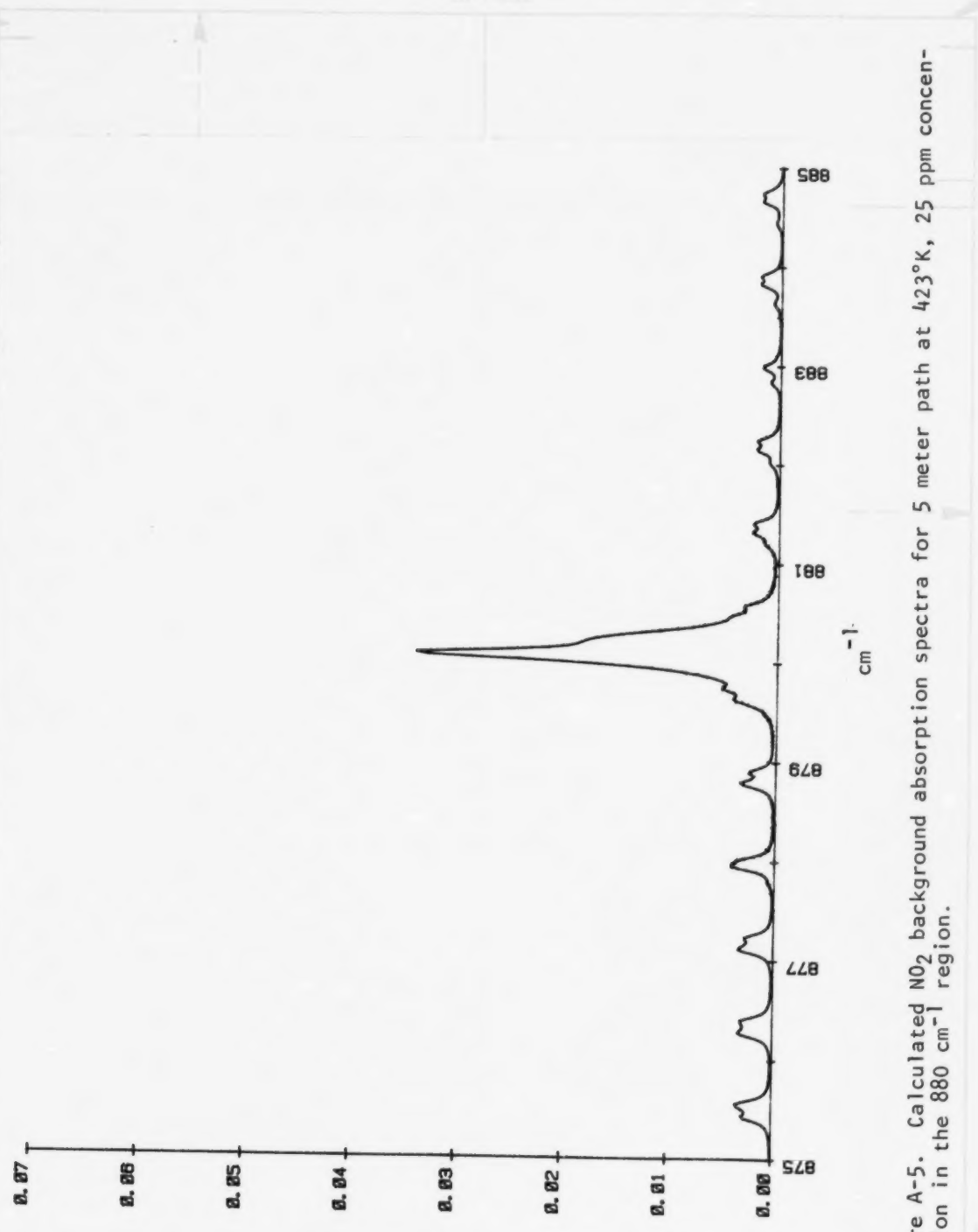


Figure A-5. Calculated $NO_2$ background absorption spectra for 5 meter path at 423°K, 25 ppm concentration in the 880 $cm^{-1}$ region.

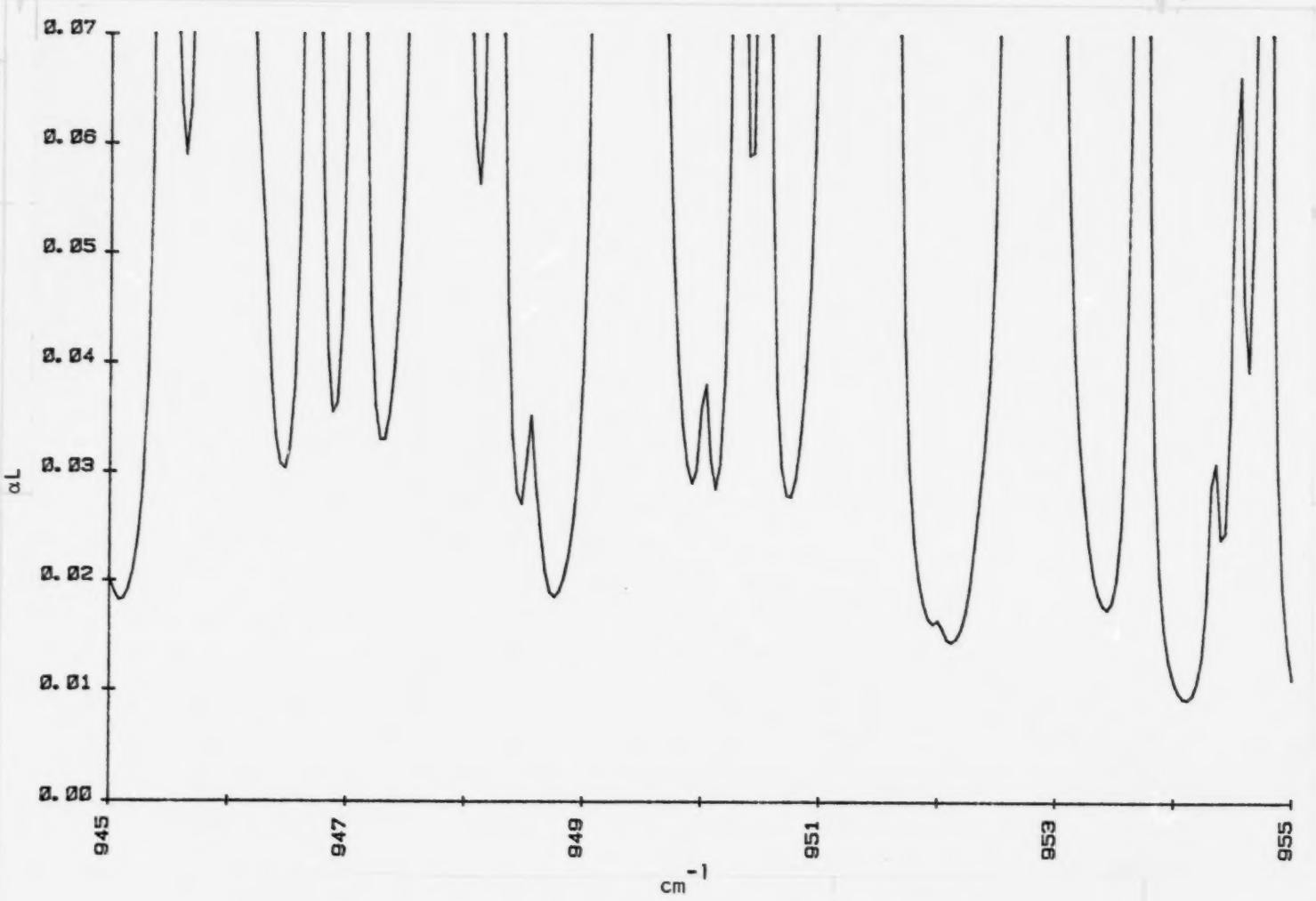


Figure A-6. Calculated $CO_2$ background absorption spectra for 5 meter path at 473°K, 114 Torr in the 960 $cm^{-1}$ region.

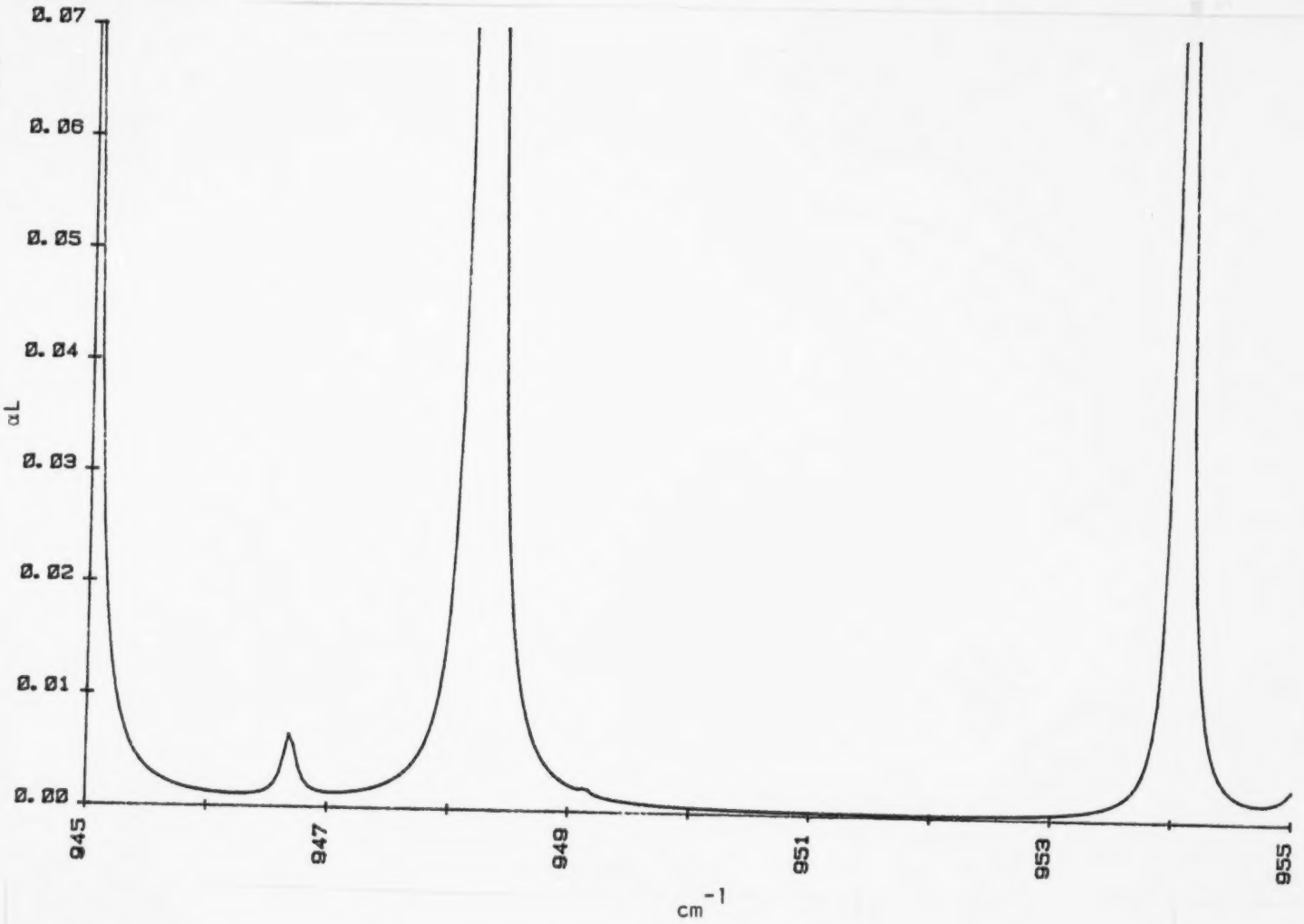


Figure A-7. Calculated $H_2O$ background absorption spectra for 5 meter path at 473°K, 91 Torr in the 950 $cm^{-1}$ region.

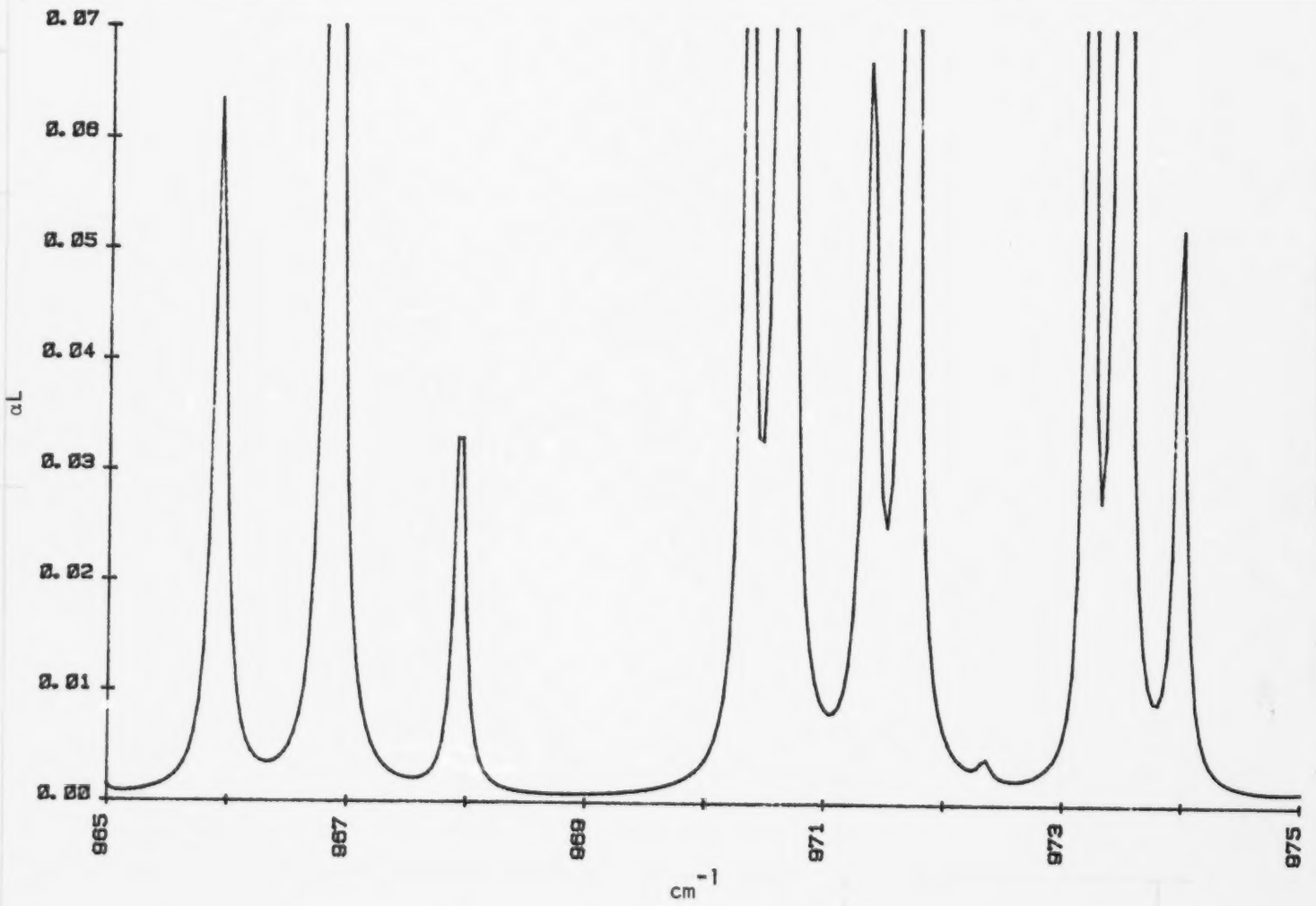


Figure A-8. Calculated $H_2O$ background absorption spectra for 5 meter path at 473°K, 91 Torr in the 970 $cm^{-1}$ region.

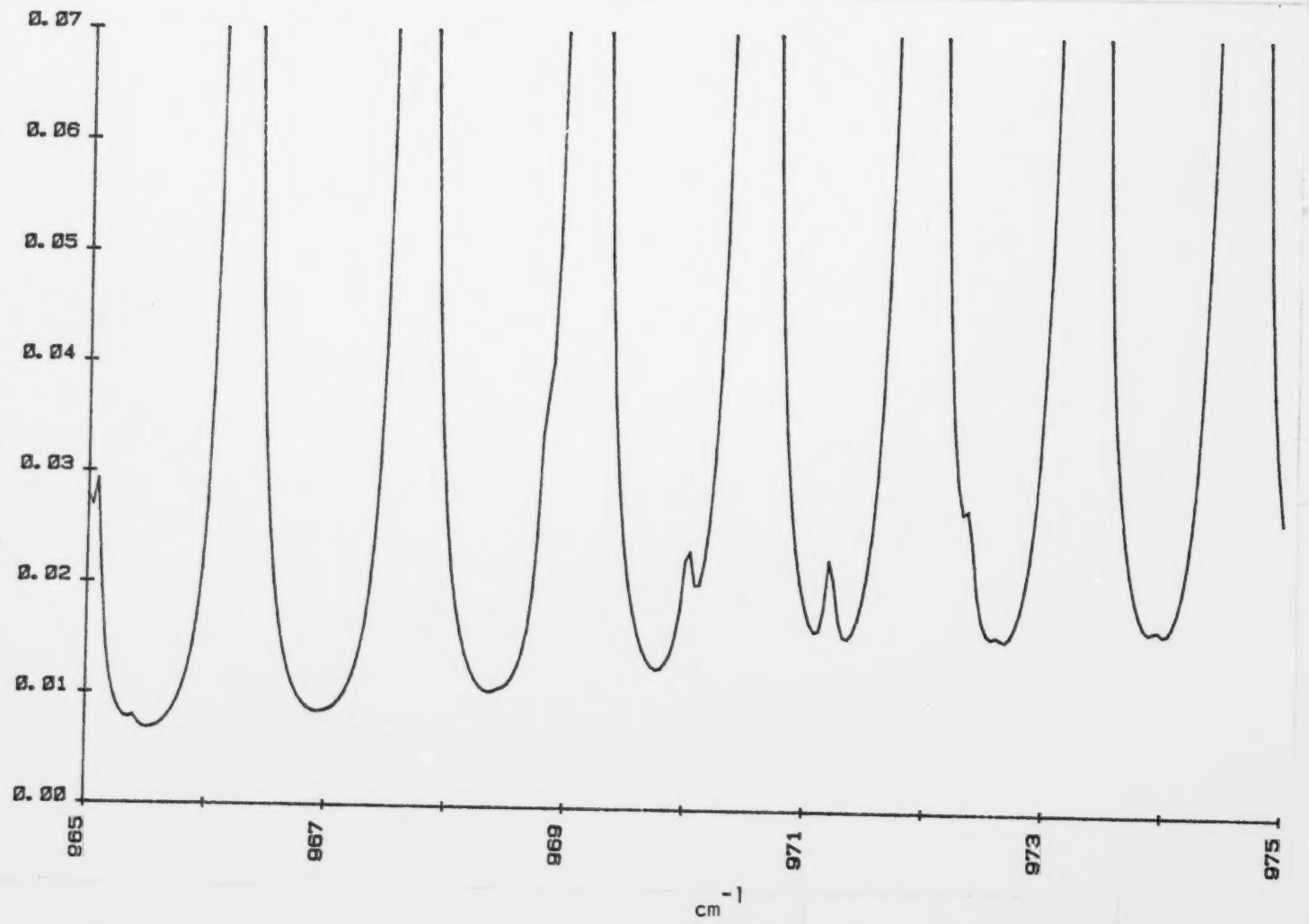


Figure A-9. Calculated $CO_2$ background absorption spectra for 5 meter path at 473°K, 114 Torr in the 970 $cm^{-1}$ region.

**TECHNICAL REPORT DATA**
*(Please read Instructions on the reverse before completing)*

| 1. REPORT NO. | 2. | 3. RECIPIENT'S ACCESSION NO. |
|---|---|---|
| EPA-600/2-80-174 | | PB 80 202690 |

**4. TITLE AND SUBTITLE**
A TUNABLE DIODE LASER STACK MONITOR FOR SULFURIC ACID VAPOR

**5. REPORT DATE**
AUGUST 1980 ISSUING DATE.

**6. PERFORMING ORGANIZATION CODE**

**7. AUTHOR(S)**
Edwin F. Pearson
Arlan W. Mantz

**8. PERFORMING ORGANIZATION REPORT NO.**

**9. PERFORMING ORGANIZATION NAME AND ADDRESS**
Laser Analytics, Inc.
Bedford, Massachusetts 01730

**10. PROGRAM ELEMENT NO.**
C07A1D/05-0390 (FY-80)

**11. CONTRACT/GRANT NO.**
68-02-2990

**12. SPONSORING AGENCY NAME AND ADDRESS**
Environmental Sciences Research Laboratory -- RTP, NC
Office of Research and Development
U.S. Environmental Protection Agency
Reserach Triangle Park, NC 27711

**13. TYPE OF REPORT AND PERIOD COVERED**
Final 9/78-3/80

**14. SPONSORING AGENCY CODE**
EPA/600/09

**15. SUPPLEMENTARY NOTES**

**16. ABSTRACT**

A field prototype instrument for continuous in-situ monitoring of sulfuric acid vapor in industrial smoke stacks has been developed. The method of detection is dual wavelength differential absorption in the infrared. Two tunable diode lasers are locked to two specific frequencies that provide analytical and background absorption information. The difference between the analytical and background absorption yields the net absorption due to sulfuric acid.

Calibration of the monitor depends upon a precise determination of the differential absorption coefficient for the analytical and background frequencies. Measurements made as a part of this program yield a value of $12.2 \times 10^{-4}$ $ppm^{-1}$ $m^{-1}$ and tend to resolve the discrepencies between previously published values. Temperature gradients in the absorption cells severely influenced previous measurements.

The monitoring system was field tested at a 650 MW electrical generation plant burning high sulfur oil of Venezuelan origin. The excess air supplied to the boiler combustion chamber was varied from 0.5 to 1.5 percent. Measured baseline concentration of sulfuric acid ranged from 3 to 25 ppm. As the excess air was stepped up from 0.5 to 1.5 percent, the average measured increase in concentration was 39 ppm. The system gave consistent results during the brief test period.

**17. KEY WORDS AND DOCUMENT ANALYSIS**

| a. DESCRIPTORS | b. IDENTIFIERS/OPEN ENDED TERMS | c. COSATI Field/Group |
|---|---|---|
| Air pollution<br>* Sulfuric acid<br>* Vapors<br>* Flue gases<br>* Monitors<br>Infrared lasers<br>Field tests | Tunable diode lasers | 13B<br>07B<br>07D<br>21B<br>20E<br>14B |

| 18. DISTRIBUTION STATEMENT | 19. SECURITY CLASS *(This Report)* | 21. NO. OF PAGES |
|---|---|---|
| RELEASE TO PUBLIC | UNCLASSIFIED | 71 |
| | 20. SECURITY CLASS *(This page)* UNCLASSIFIED | 22. PRICE |

EPA Form 2220-1 (9-73)